CHAPTER-II

Effect of Preparative Parameters on Structural, Morphological, Electrical and Optical Properties of Nanocrystalline ZnO Thin Films

2.1 Introduction

As discussed in section (A) of chapter one, the advanced spray pyrolysis technique is modified from the conventional spray pyrolysis system by retaining all its previous advantages [1]. However, the basic structure is completely changed. In this technique, it is planned to complete the reaction in the reaction chamber and the final product will be deposited on the substrates, which are kept at a low temperature. Thus, similar to most of above deposition techniques and especially the spray pyrolysis, this novel advanced spray pyrolysis has its own process parameters that have profound effects on the physical and gas sensing properties of ZnO thin films and hence need to be optimized properly. Therefore, in the present study, due to their crucial role in controlling many properties, the core temperature (reaction temperature), substrate temperature, thickness dependence and layer by layer (LBL) deposition dependence of structural, morphological, electrical, optical and gas sensing behavior of undoped ZnO thin films was studied and reported in this chapter. Physical properties of nanocrystalline ZnO thin films, including electrical resistivity, through the resulted microstructure were carefully examined.

2.2. Experimental Details

Deposition of ZnO films using advanced spray pyrolysis method includes the substrate cleaning, thermogravimetric analysis of selected precursor, solution preparation and deposition etc. The preparative parameters were optimized in order to get nanocrystalline and feasible films for gas sensor application. The ZnO films were characterized using various techniques in order to get information on their structural, surface morphological, electrical and optical properties.

2.2.1. Substrate Cleaning

Substrate cleaning plays an important role in the deposition of zinc oxide thin films. Sufficient cleaning of the substrate and proper surface treatment prior to the deposition are essential for making uniform and crack-free films; as the contaminated surface provides nucleation sites facilitating growth resulting into non-uniform films with different orientation and impurities. It should be emphasized that the defect formation and density should always depend on the cleanness of the production environment and the effective surface cleaning/treatment method should be chosen specifically for a particular substrate. The glass microslides supplied by 'Blue Star' of dimensions 75 mm × 25 mm × 1.35 mm have been used as the substrates. The following procedure has been adopted for cleaning the substrates:

a) The glass slides were washed with detergent and distilled water,
b) Then boiled in concentrated chromic acid (0.5 M) for ½ hr and kept in it for ½ hr,
c) The substrates were washed with double distilled water,
d) The substrates were ultrasonically cleaned for 30 min,
e) Then, the substrates were exposed to the methanol vapors for 15 minutes and
f) Finally, the substrates were dried, degreased in AR grade acetone and were used for deposition.

2.2.2. TGA-DTA Analysis of Zinc Acetate

Phase transformations and mass loss events occurring during heating of zinc acetate (Thomas Baker, 99.5%) powder were investigated via simultaneous differential thermal (SDT-2960) analyzer (TA Instruments Inc., New Castle, DE). The transformation temperatures determined by TGA were also done using a model 2960 simultaneous thermogravimetric analyzer (TA Instruments, Newcastle, DE).

The thermogram recorded for zinc acetate powder is shown in figure 2.1. The thermal evolution in oxygen ambient occurs in four successive stages with weight losses for which the inflection point coincides with the temperature corresponding to the endotherms and exotherms in DTA trace. The weight loss of

precursor zinc acetate [Zn $(CH_3COO)_2 \cdot 2H_2O$] begins at 333K. Initially, weight loss of 16.43% of zinc acetate in the temperature range of 333-373K was observed (Step I). This is indicated by the endothermic peak at 368K due to the evaporation of physisorbed water from the precursor. This is followed by a slow decay of TGA curve in the temperature range of 373-513K (Step II). The rapid decay in TGA curve was takes place during 373-598K (Step III). During step II & III; total weight loss was 60.15%. These consequents weight losses are attributed to the decay leading to the decomposition of acetate groups. A further weight loss approximately at the temperature of 598K coincides with an exothermic peak indicating the formation of ZnO phase and becomes stable after the temperature of ~600K. After ~600K the TGA trace is stable with no further weight loss indicating the decomposition of zinc acetate formation of stable ZnO phase. In the DTA trace, the exothermic peak signifies the crystallization or phase formation [2].

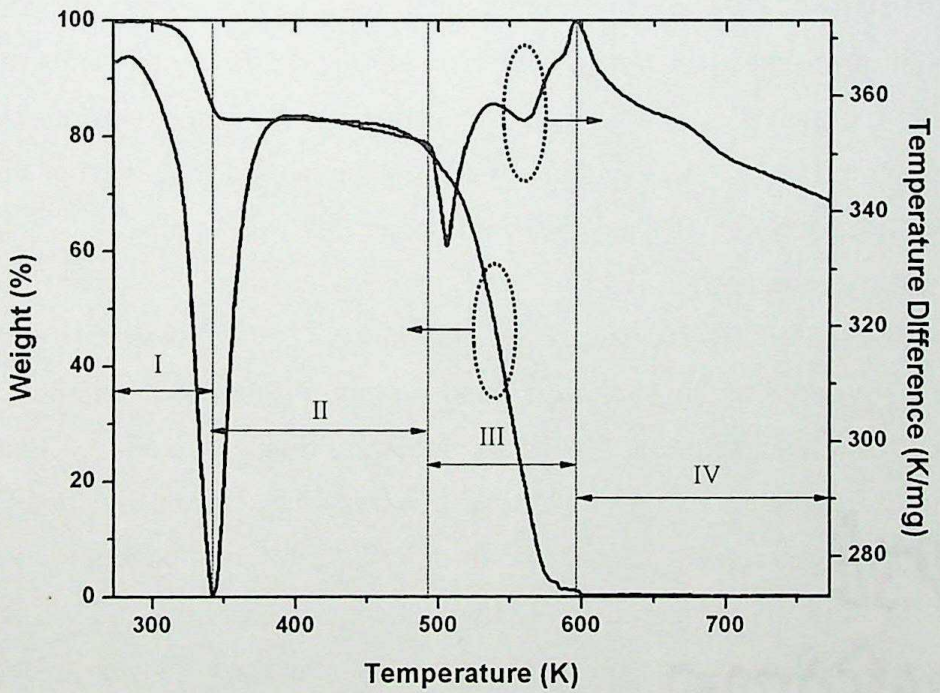


Figure 2.1: *TGA-DTA curves for analyzing decomposition behavior of Zinc Acetate dihydrate.*

For the first endothermic peak,

$$Zn(CH_3COO)_2.2H_2O \xrightarrow{\Delta} Zn(CH_3COO)_{2liq} + 2H_2O_{vapor}\uparrow \text{ (Physisorbed Water)} \text{ ---------- } (2.1)$$

For the second endothermic peak,

$$Zn(CH_3COO)_{2liq} + 2H_2O_{liq} \longrightarrow Zn(CH_3COO)_{2solid} + 2H_2O_{vapor}\uparrow \text{ (Chemisorbed Water)} \text{ ------ (2.2)}$$

For the exothermic peak,

$$Zn(CH_3COO)_{2solid} \xrightarrow[Oxidation]{\Delta} ZnO_{solid} + + 2(CH_3COO)\uparrow + 2(CH_3)\uparrow + 2(CO_2) \text{ ---------- (2.3)}$$

2.2.3. Deposition of Zinc Oxide Thin Films

The schematic experimental set up of advanced spray pyrolysis method for ZnO thin film deposition is shown in figure 1.2. It consists of mainly a reaction chamber, a substrate heater, temperature controllers and nozzle assembly.

Zinc oxide films were deposited by using a non-aqueous solution (100ml) of 0.1M concentration of high purity zinc acetate [$Zn(CH_3COO)_2 \cdot 2H_2O$] (Thomas Baker, India) dissolved in methanol. The solution was sprayed through a glass nozzle onto the ultrasonically cleaned glass substrates. Compressed air at a pressure of 10 LPM is used to regulate the solution spray rate at ~6 ml min^{-1}. For the study of effect of core temperature (reaction chamber temperature) on ZnO film properties [section (A)], by maintaining the substrate temperature at 473 K, constant ZnO films were deposited at different reaction chamber temperature (548 to 648 K at steps of 25K). Whereas, study of effect of substrate temperature [section (B)] on ZnO film properties was carried out by varying substrate temperature (423 to 523K at steps of 50K) at a constant core temperature 598K. To investigate the film thickness effect [section (C)], the ZnO films were deposited by spraying various volumes (50ml to 200ml at a step of 50ml) of spraying solution at constant substrate temperature (473K) and core temperature (598K). Furthermore for the ZnO layer by layer deposition [section (D)], first layer was deposited by spraying 100ml solution onto glass at a constant substrate temperature (473K) and core temperature (598K) and then allowed to cool down at room temperature. For the second layer, as-deposited single layered zinc oxide thin films were used as substrates and same deposition procedure was carried out by maintaining same deposition conditions. For third and fourth layers, same process was repeated so that the previous zinc oxide under-layer will act as substrate for the subsequent over layer. Throughout the experimentation, the both the substrate and core temperature were controlled

using electronic temperature controllers. Hazardous gases evolved during the thermal decomposition were expelled out.

2.2.4. Characterization Techniques

The structural investigations of the ZnO thin films were carried out using a X-ray diffractometer (German make Bruker axs D-8 Advance Model) with Cu K_α (λ = 1.54 Å)] radiation operating at 40 kV and 30 mA and step size of 0.11. Surface morphology of the ZnO thin films, grain size and distribution of grains were examined by scanning electron microscope (SEM, Model: JEOL JSM-6360) or field emission scanning electron microscopy (FE-SEM, Model: JSM-6701F). To determine the thickness of the ZnO film, the cross-sectional view FESEM micrographs of the as-deposited ZnO films were obtained. Cross-sectional FESEM specimens were made by carefully cleaving glass substrates with ZnO films deposited on the surfaces, while protecting the surfaces/films with soft filter papers. Film thickness was measured from cross-sectional SEM images, and the mean of number of measurements made at different locations were reported for each film. Additionally, film thickness was verified using AMBIOS-XP-1 surface profilometer. Furthermore, the surface morphology and surface roughness of the films was observed at room temperature by atomic force microscopy (AFM, Digital Instrument, nanoscope III) respectively. AFM images were collected in contact mode on a molecular imaging system using a silicon nitride cantilever. Feature heights, roots mean square (RMS) surface roughness, and surface area was calculated using digital instruments software. Optical absorption (normal incidence) measurements of the films were made at room temperature in the spectral range of 350–850 nm using a UV–VIS spectrophotometer (Shimadzu 1800 model). The electrical resistivity of the ZnO thin films were measured by home made two-probe resistivity unit. Colloidal silver paste was used for ohmic contacts. Photoluminescence (PL) spectra were obtained using a closed-cycle liquid helium cry generator (APD, SH-4, USA), a spectrometer (f = 0.5 m, Acton Research Co., Spectrograph 500i, USA) and intensified photodiode array detector (Princeton Instrument co., IRY1024, USA). All spectra were measured at room temperature with an Ar^+ ion laser as a light source using an excitation wavelength of 325 nm. For measurement of response to gases, the sensors were loaded in an airtight housing having a volume of 250

cm^3. A measured quantity of gas at 1000 ppm concentration was introduced in the housing using a syringe and resistance of the samples was measured as a function of time.

2.3 Results and Discussion

Non-aqueous solution of zinc acetate dissolved in methanol, when sprayed over the preheated substrates through the reaction chamber, pyrolytic decomposition of solution takes place and constituent reacts to result into zinc oxide. The possible chemical reaction of ZnO film formation from zinc acetate solution as follows [3],

$$Zn(CH_3COO)_2.2H_2O + 2\,CH_3OH \xrightarrow{\Delta} ZnO + 2(CH_3COCH_3) + 3H_2\uparrow + O_2\uparrow \text{ ---------- (2.4)}$$

The films deposited onto the amorphous glass substrates were mirror smooth, uniform and well adherent to the substrate.

Section (A): Effect of Core Temperature (reaction chamber temperature)

2.3. (A) 1. X-ray Diffraction studies

The influence of the core temperature on the crystalline state of the films has been studied using X-ray diffraction (XRD). Figure 2.2 shows the XRD patterns of films grown at different core temperatures. It is evident from this figure that structural properties of the ZnO films largely depend on core temperature. The films grown at low core temperature (< 573K) are largely amorphous in nature incorporated with an undecomposed acetate group as expected from TGA-DTA analysis of zinc acetate in section 2.2.2, while the films grown at higher temperatures (≥ 598K) are crystalline in nature. Though some very feeble peaks are observed for films grown at 548K and 573K core temperatures, those are so pathetic that difficult to discriminate from the noise. Four well-defined peaks, identified as the (100), (002), (101) and (103) diffraction planes of ZnO, are clearly observed for the ZnO film obtained at 598K core temperature, indicating the polycrystalline wurtzite structure of ZnO [JCPDS No. 05-0664]. The film deposited at 598K is dominantly oriented along (002) plane; however film preferential orientation decreases with further increase in core temperature. This behavior of XRD pattern is in good agreement with the literature data [4].

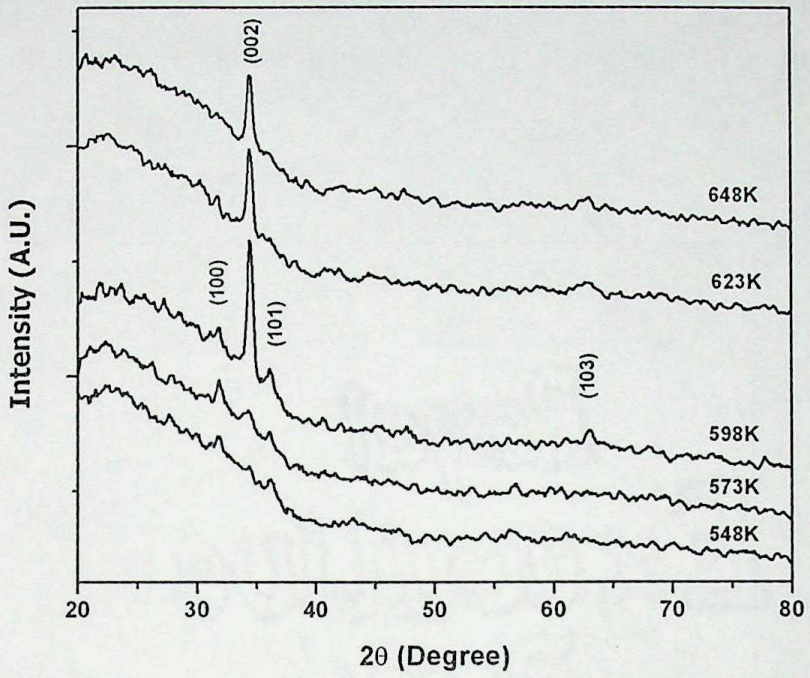


Figure 2.2: *XRD patterns of ZnO thin films prepared at different core temperatures.*

The mean crystallite size D was calculated from the full-width at half-maximum (FWHM) using Scherrer formula [5]:

$$D = \frac{0.9\lambda}{\beta \cos\theta_B} \text{ ---------- (2.5)}$$

where λ is radiation wavelength (1.54 Å), β is FWHM of the diffraction peak and θ_B is a diffracting angle. An estimated crystallite size of untreated films was in the range ~10 to ~20 nm. From figure it is seen that the average crystallite size increases with increase in core temperature and the ZnO film deposited at core temperature 598K is comprised of the crystallites of highest average size ~20 nm; while for the higher core temperature the crystallite size slightly decreases. In addition, to get more information on the amount of defects in the films the dislocation density was calculated using following formula using the simple approach of Williamson and Smallman [6],

$$\delta = \frac{1}{D^2} \text{ ---------- (2.6)}$$

The δ values are also shown in figure 2.3. Larger D and δ values indicate better crystallization of the films. As can be seen in Figure 2.3, the better crystallization turned out to be for film prepared at 598K in accordance with to the D and δ values.

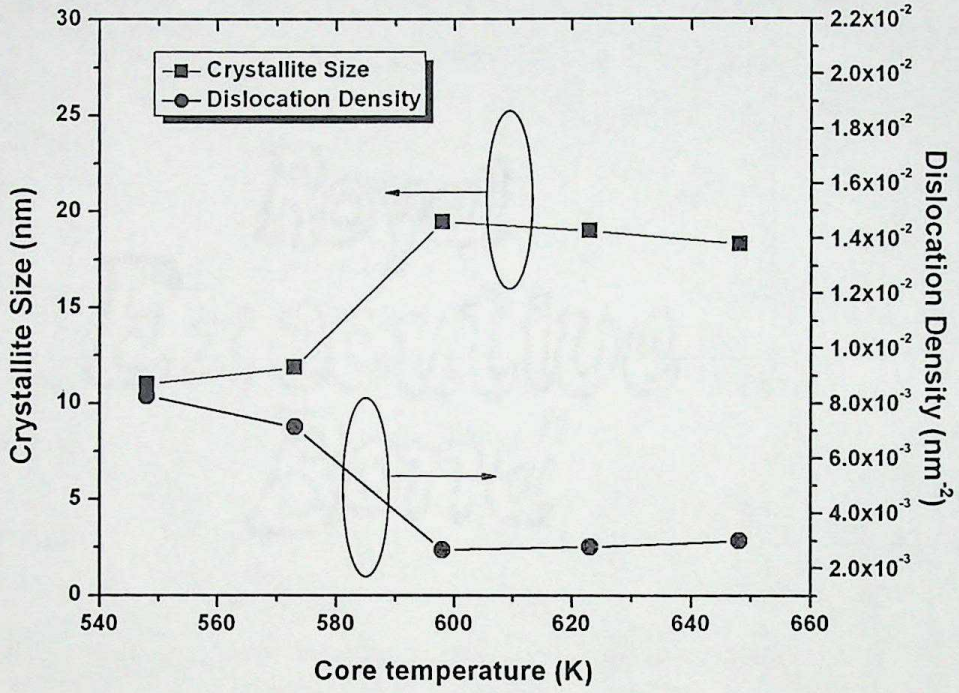


Figure 2.3: *Crystallite size and dislocation density in ZnO thin films as a function of core temperature.*

2.3. (A) 2. Surface Morphology

It is known that the surface properties of the sensor films directly influence their sensing performance. For example, the increase in surface grain size of the films leads to a decrease in the surface area to be exposed to the gas and thus results in a decrease in the response of gas sensor. Therefore, it is very important to investigate the surface morphology of the films. Herein, to investigate the surface morphology, film thickness and RMS roughness of ZnO films, field emission scanning electron micrograph (FESEM) and atomic force micrograph (AFM) images were studied.

2.3. (A) 2.1 Field Emission Scanning Electron Micrograph (FESEM) Study

Figure 2.4 (a)-(e) shows the plain view FESEM micrographs of ZnO films prepared at various core temperatures.

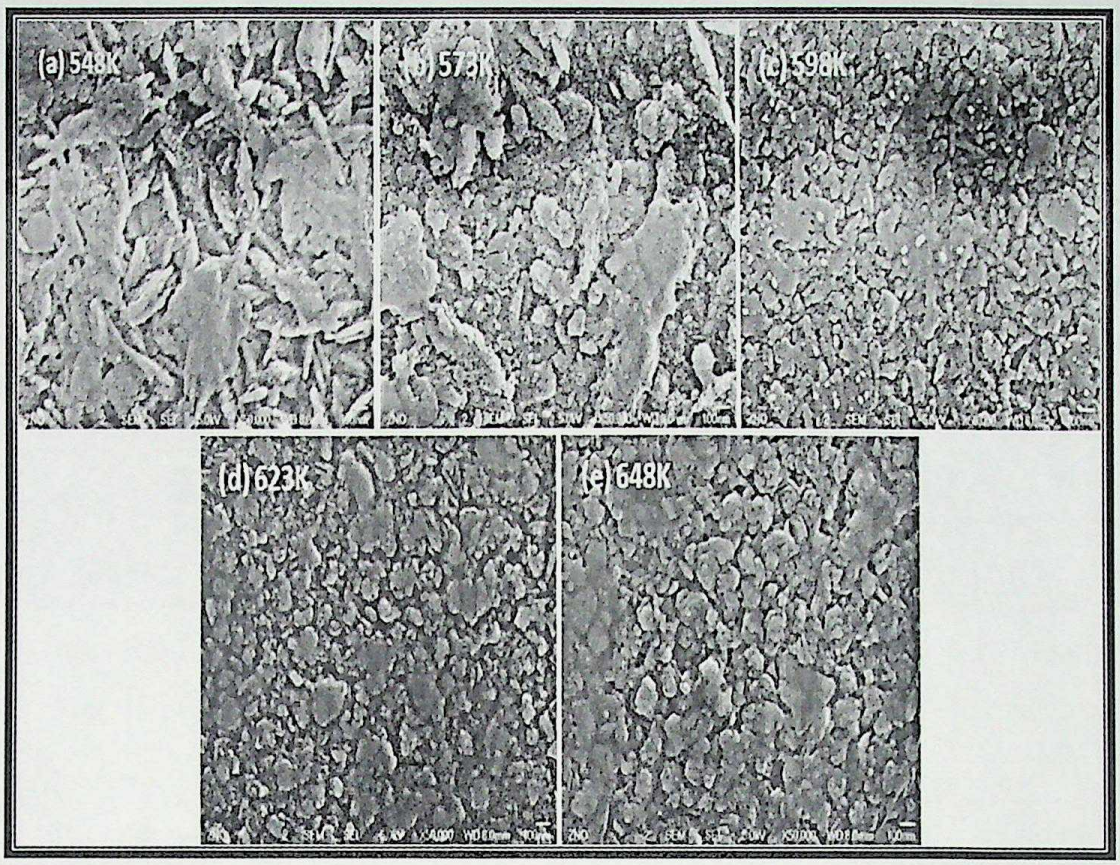


Figure 2.4: *Plain view FESEM micrographs for ZnO films prepared at various core temperatures: (a) 548K, (b) 573K, (c) 598K (d) 623K and (e) 648K.*

It is found that the whole surface is rough and uneven for the films prepared at low temperature (<573K), combining with the results of XRD patterns discussed previously, which is assigned to the incomplete crystallization. However, at high temperature (≥598K), the complete crystallization is observed and the surface is smooth. Note that no cracks are observed on large scan area for all samples. The films are continuous and in fact consist of grains. The film prepared at 598K shows highly compact surface supporting the (002) intensity maxima observed for same sample during XRD studies. At 623K and 648K, it appears that small crystallites coalesce together to make larger crystallites and the grain size is in inhomogeneous distribution. Some voids in between agglomerates can be seen for the samples prepared at 623K and 648K. These agglomerates are composed of many grains with sizes somewhat bigger than crystallite sizes as measured from X-ray diffraction patterns. The observed difference may be associated with the fact that we have

not considered the broadening of the peak due to layer stress on calculating the crystallite sizes.

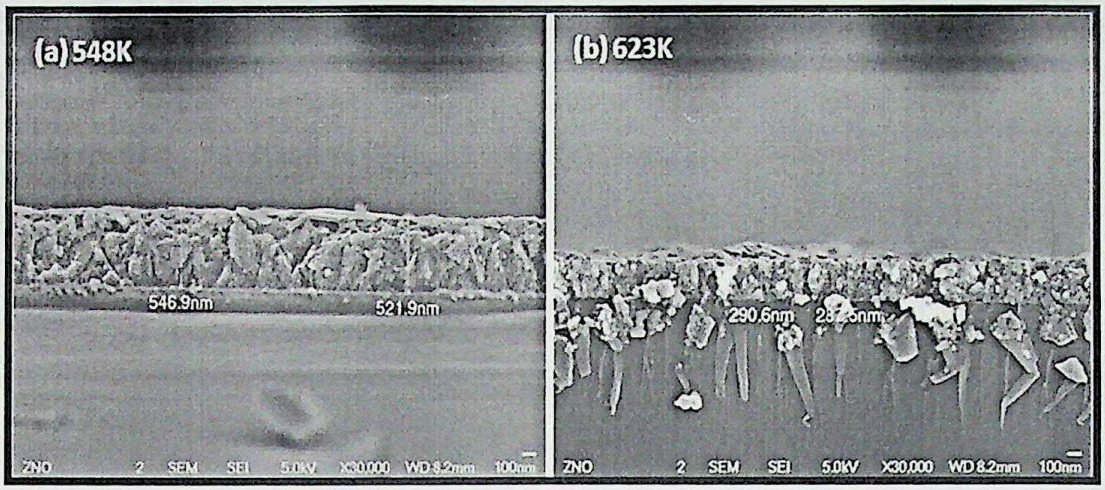


Figure 2.5: *Typical cross-sectional view FESEM micrographs for ZnO films prepared at various core temperatures: (a) 548K, and (b) 623K.*

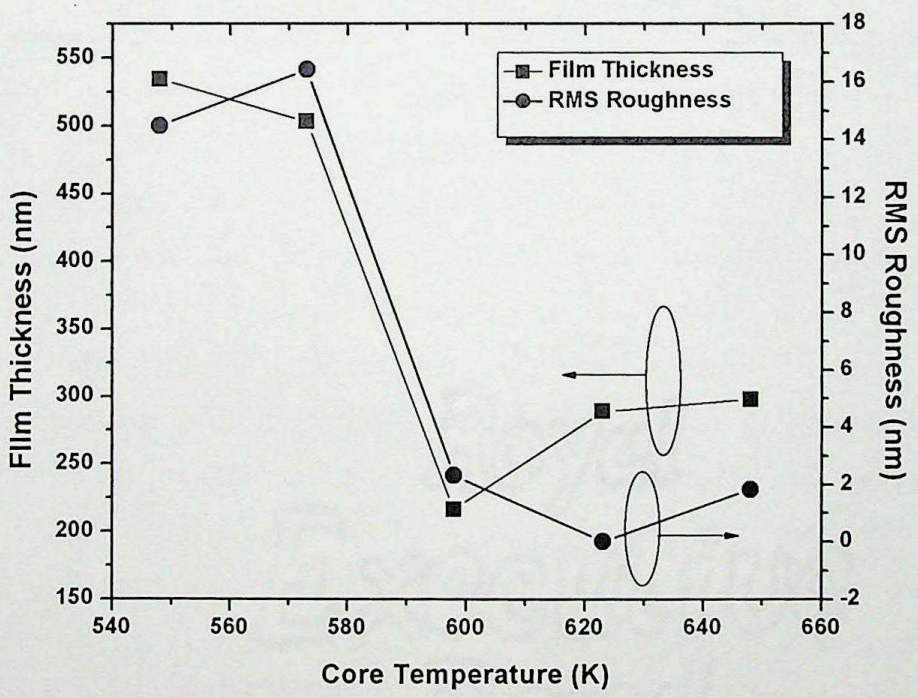


Figure 2.6: *Variation of film thickness (nm) and RMS roughness (nm) with core temperature.*

Further, the thickness of the films was measured at different positions from the cross-sectional FESEM images. Figs. 2.5 (a) and (b) presents typical cross sectional view FESEM micrographs of ZnO films prepared at 548K and

623K. Film thicknesses measured from the cross sectional FESEM image are found to be within the range of 216 nm to 535nm. Thickness is observed to be above 500nm for the samples deposited at ≤573K due to amorphous like deposits resulting from the incomplete thermal decomposition of the reactants; whilst the core temperatures ≥598K leading to crystallization offer decreases the thickness well below 300nm. The rapid change in thickness of film deposited at 573K and 598K may be due to major grain growth, which is consistent with the analysis of XRD results above. The variation of the film thickness with core temperature is represented in figure 2.6.

2.3. (A) 2.2 Atomic Force Micrograph (AFM) Study

The AFM images shown in figure 2.7 illustrate the effect of the core temperature on the surface morphology of ZnO thin films. Here the scanning area of the AFM image in figure 2.6 is 3×3 μm^2. The AFM images clearly show dense surface morphology and the result of the analysis indicates that the core temperature can influence the surface roughness and grain size. The bright area in the 2D micrographs is the overgrown clusters of ZnO crystallites indicating the well developed grain morphology. The apparent size of the grains from the surface images is higher than the values calculated from the XRD measurements, indicating that these grains are probably an aggregation of crystallites.

The variation of root mean square (RMS) surface roughness for the ZnO film with core temperature estimated from AFM images is shown in figure 2.6. It is a bit high for the samples prepared at 548K and 573K attributed to the amorphous like morphology. It decreased to 0.006 nm at 623K. Such a small roughness of ZnO thin film could be explained as a consequence of a reduction in the grain size with a uniform and compact surface morphology as evidenced from the FESEM images. However for further increase in core temperature i .e at 648K the surface roughness slightly increases to 1.837 nm; which may be ascribed to the increase in evaporation rate on the surface. The observed RMS roughness values (<3nm) of the polycrystalline ZnO films deposited at 473K substrate temperature by advanced spray pyrolysis technique are much smaller than that (~40nm)of the ZnO film deposited by conventional spray pyrolysis technique; though the usual sprayed films were deposited at higher (673K) substrate temperatures [7]. Further, the obtained surface roughness is

comparable to that for the ZnO films deposited at the same substrate temperature by sophisticated technique such as RF magnetron sputtering [8]

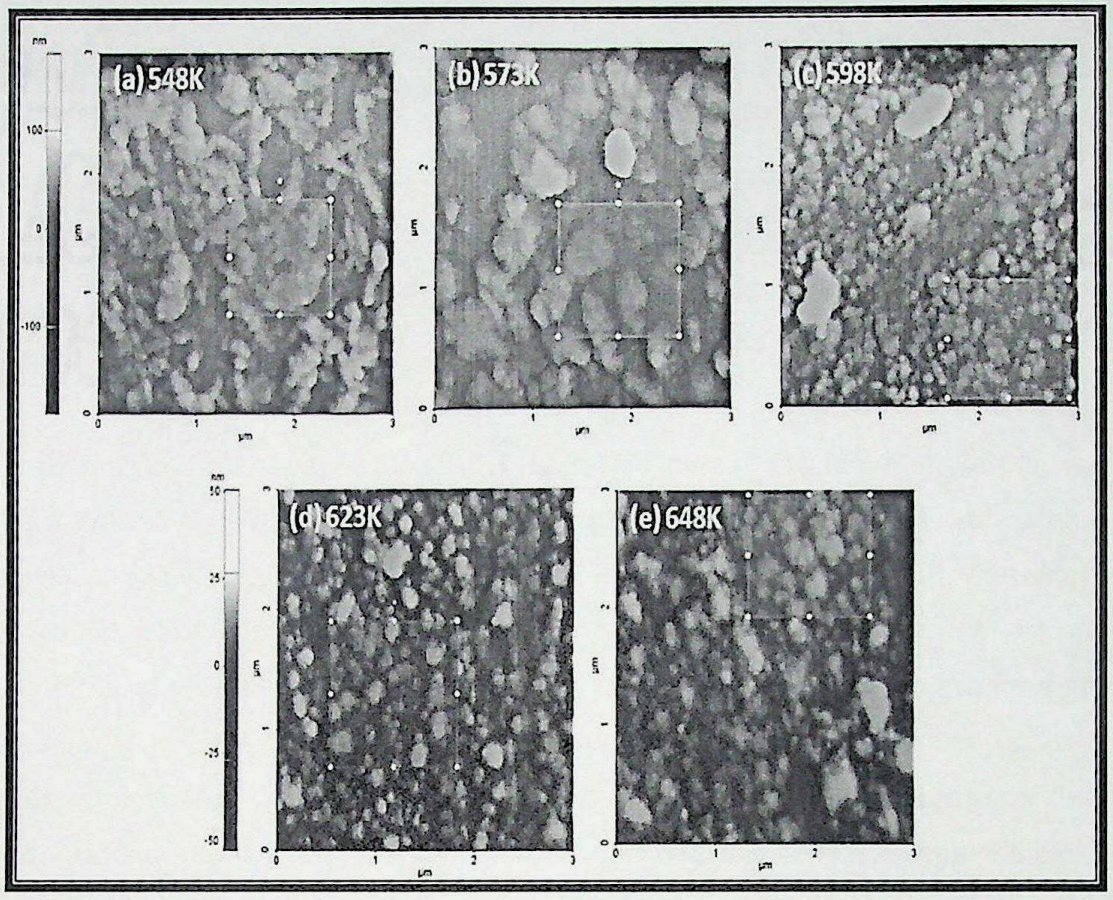


Figure 2.7: *AFM images for ZnO films prepared at various core temperatures: (a) 548K, (b) 573K, (c) 598K (d) 623K and (e) 648K.*

2.3. (A) 3. Electrical Resistivity

The electrical behavior of ZnO samples with respect to their core temperatures was examined through measurements of the electrical resistivity (ρ). In the present study, the electrical resistivity of ZnO films was measured by conventional d. c. two-probe method in the range of 300 to 600K. A Chromel-Alumel thermocouple (24 gauges) was employed to measure the temperature. The silver paste contacts of 1 mm separated by 1 cm were used to form Ohmic contacts. Ohmic behavior of the contacts are confirmed by checking the current (I)–voltage (V) characteristic across the contacts which show a linear dependence of current on applied voltage. The temperature dependence of the electrical resistivity can be described by the well-known exponential law [9],

$$\rho = \rho_0 \exp\left[-\frac{E_a}{k \cdot T}\right] \text{----------(2.7)}$$

where ρ_0 is the constant depending on the sample characteristics (structure, thickness, etc.), k is the Boltzmann constant, T is the absolute temperature, and E_a is the activation energy for electrical conduction. Activation energy is the amount of thermal energy required to release an electron from trap level to the conduction band (CB). These trap levels are the levels located few meV below the CB in the forbidden region and are nothing but the crystal defects.

A plot of ln(ρ) versus 1000/T for the advanced sprayed ZnO thin film deposited at different core temperatures shown in figure 2.8 signifies the semiconducting nature of the ZnO thin film. The room temperature resistivity was found to be of the order of 10^1 to 10^{-1} Ω-cm. This high resistivity may be due to nanocrystalline nature of the samples. Additionally, the high resistivity may also be attributed to the oxygen chemisorptions [10, 11] at grain boundaries since air was used as carrier gas during deposition and the decomposition reaction is about to complete in the ambient core of the reaction chamber. During deposition process it is somewhat expected that large numbers of oxygen molecules are chemisorbed at grain boundaries and also on the surface of the film. Because these molecules do not have time to leave the sample at the end of deposition, due to the rapid cooling effect. From figure 2.9, it is clearly seen that the resistivity of the film deposited at 548K core temperature has two distinct conduction mechanisms. The transition from a straight line region with a low slope to one with a higher slope as temperature is increased implies involvement of more than one conduction mechanisms. These two regions might be due to hydroxide and some other impurity inclusions which are a most commonly observed phenomenon. Two different slopes are thus seen in figure. While samples deposited at higher core temperatures do not show such conduction behavior of two regions. The activation energy represents the location of trap levels below the conduction band. The activation energy values were calculated from the slope of the graphs. The activation energy values are found between 0.10 eV to 0.67 eV (Inset of the figure 2.9). These activation energies may be related with the inter-crystalline barrier height separating the ZnO grains from each other and different oxygen vacancies [12]. With increasing temperature,

more charge carriers overcome the activation energy barrier and these carriers participate in the electrical conduction.

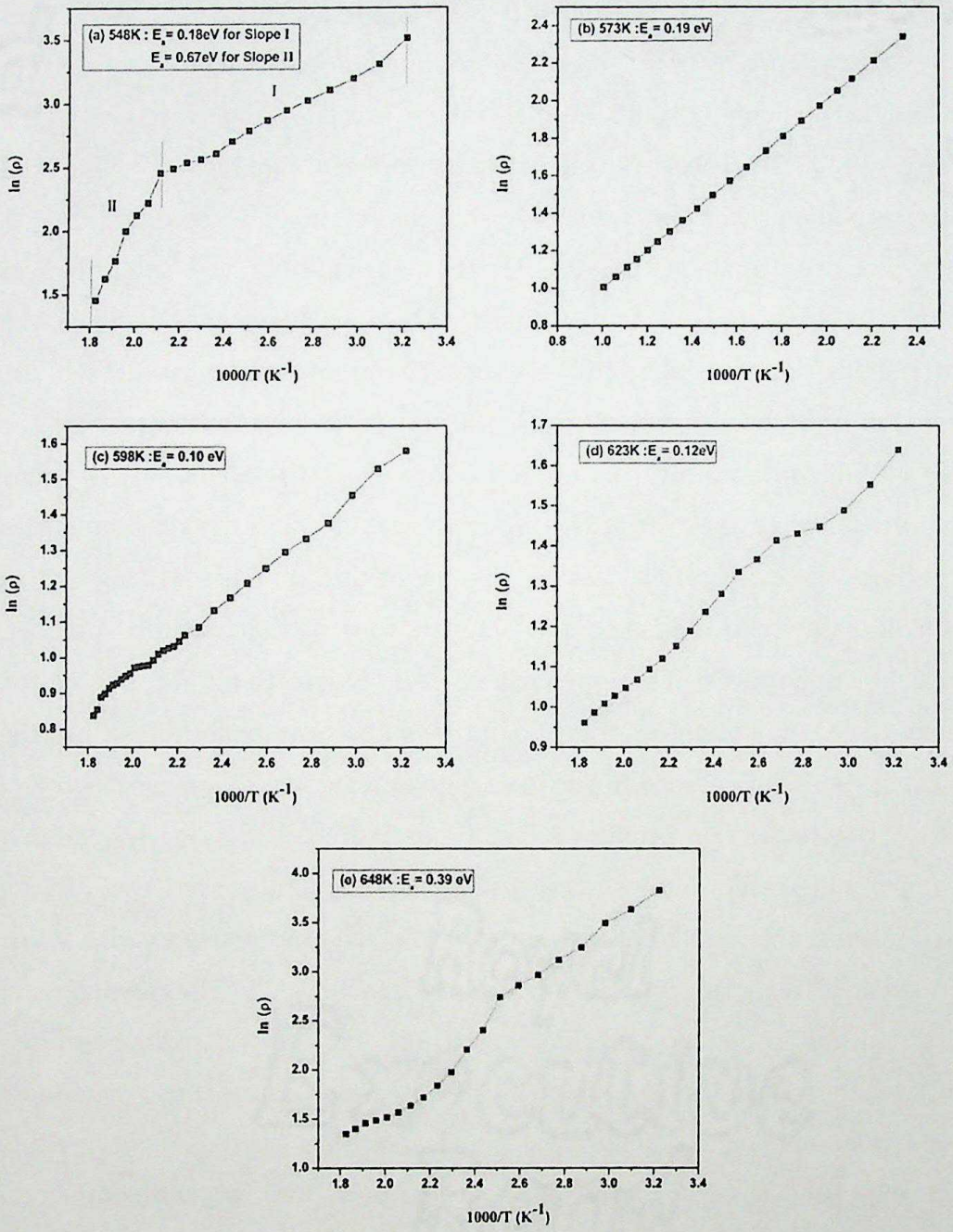


Figure 2.8: *The variation of ln (ρ) with (1000/T) of ZnO thin film prepared at various core temperatures.*

2.3. (A) 4. Optical Absorption Studies

Figure 2.9 presents the UV-visible transmission spectra of ZnO thin films recorded in the visible region of 350–1100 nm, as a function of the core

temperature. The inset shows the optical absorption spectrum vs. wavelength. Herein, the films were found to be highly transparent in the visible wavelength region with an average transmittance of 83% at 550nm, with a sharp fall-off for wavelengths shorter than 380 nm, characteristics of high quality ZnO films. The optical properties of films are influenced by both the thickness and surface morphology of ZnO films. The smoother surface morphology and less grain boundary density the films has, the higher the transmittance is. The lower transmittance at lower core temperature (≤573K) may be attributed to the increased photon scattering by crystal defects and large surface roughness. An enhancement in the transmittance of zinc oxide films can be accredited to the removal of organic and hydroxide species on the film.

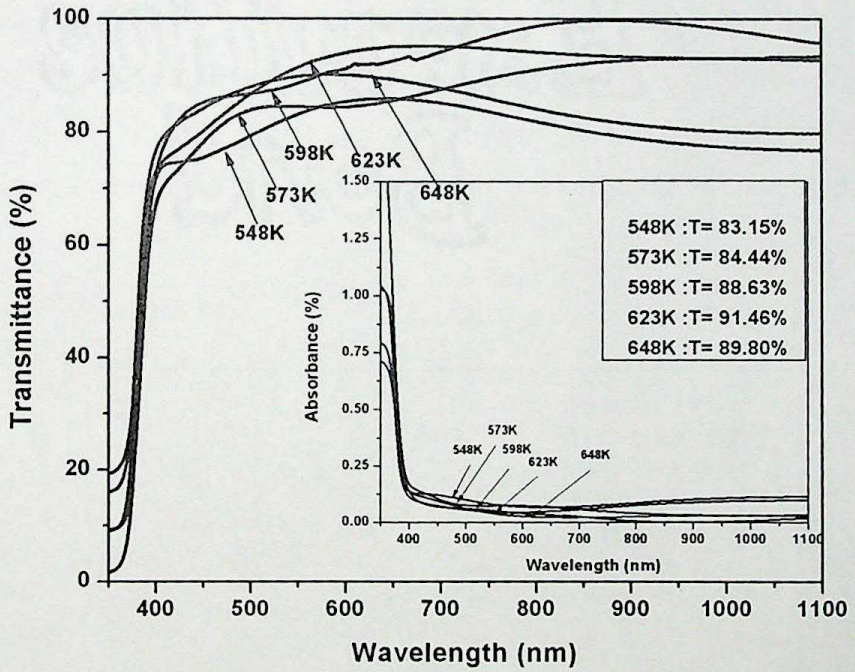


Figure 2.9: *Optical transmission spectra of ZnO films prepared at different core temperature.*

In order to better investigate the influence of the core temperature on the absorption of the ZnO films, the recorded transmission spectra were employed for the determination of the optical energy gap E_g. Assuming a direct transition between the edges of the valence and the conduction band, the variation of the

absorption coefficient α with the photon energy hν can be given by the following equation:

$$\alpha = \frac{A(h\nu - E_g)^{1/2}}{h\nu} \quad \text{---------- (2.8)}$$

Tauc's plot [13] of $(\alpha h\nu)^2$ as a function of the energy of incident radiation has been shown in figure 2.10. The energy band gap is obtained from intercept of the extrapolated linear part of the curve with the energy axis and the band gap is observed to vary in between ~3.27 eV to ~3.33 eV. However, this value is less than that of the bulk ZnO films (3.37 eV). Initially with increase in core temperature from 548K to 598K the band gap decreases from ~3.33eV to ~2.27eV; however for further increase in core temperature up to 648K band gap again increases to ~3.32eV. Such optical band gap behavior may be attributed to the variation in the film thickness as well as the deviation of the film crystallinity [14]. The blue shift of band gap for the films deposited above 598K is due to an electron confinement effect related with the crystallite size in the films [15]. These observed values of optical band gap are in good agreement with the previous reports by others [16, 17]

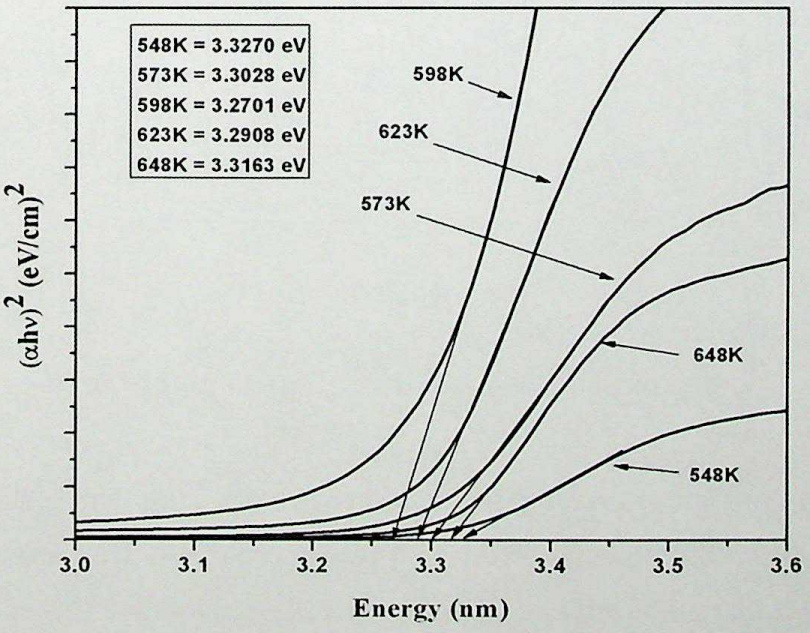


Figure 2.10: *The plot of $(\alpha h\upsilon)^2$ vs. hυ for Zn0 films deposited at different core temperatures.*

Section (B): Effect of substrate Temperature

2.3. (B) 1. X-ray Diffraction studies

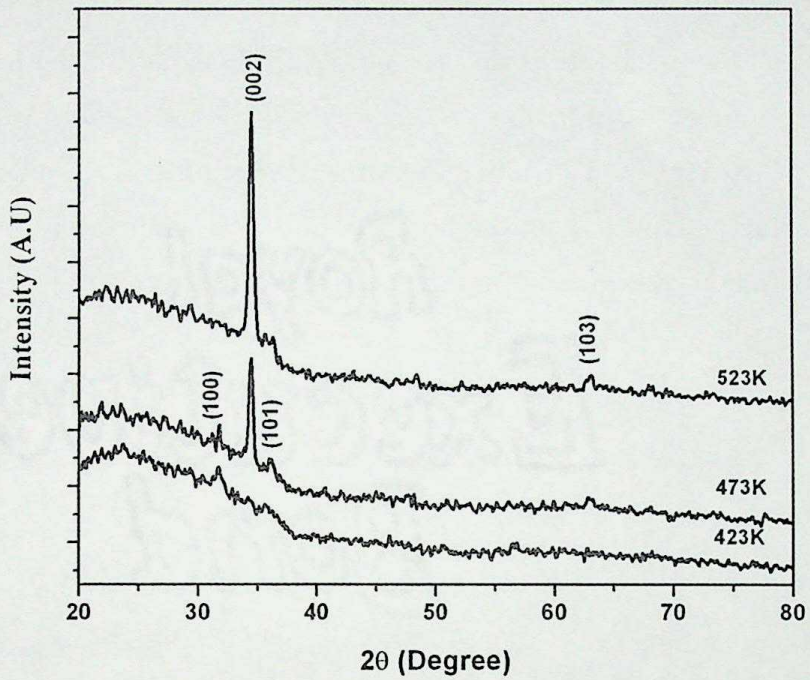


Figure 2.11: *XRD patterns of ZnO thin films grown at different substrate temperatures.*

The X-ray diffraction patterns of ZnO film deposited at different substrate temperatures are shown in figure 2.11. It is evident from this figure that structural properties of the ZnO films largely depend on substrate temperature. Interestingly, the films grown at low substrate temperature (<473K) shows some crystalline nature with a weak reflection along (100) plane, while the films grown at high temperatures (≤473K) exhibit a preferential orientation along (002) direction. However, the comparatively weak (100), (101) and (103) diffraction planes of ZnO, are also observed in patterns, indicating the polycrystalline wurzite structure of ZnO [JCPDS No. 05-0664]. The intensity of the (002) peak increases with increase in substrate temperature. The intensity of ZnO (002) peak in the XRD patterns is mainly determined by the number of crystallites with the c-axis orientation in the ZnO films. During the deposition, the atomic kinetic energy is mainly determined by substrate temperature. As compared to 423K, therefore, at a relatively higher substrate temperature viz.

473K and 523K, the atoms on the film surface can move quickly to look for the lowest energy sites and form the low energy structure i. e. the high substrate temperature enhances the mobility of the atoms on the surface and increases thermodynamic stability. These modifications suggest that the c-axis orientation and the crystallinity of the films become better, evidently, with the increase of the substrate temperature. In the present investigation it is noteworthy that, though the films deposited at low substrate temperatures such as 423K and 473K, the films exhibits good adherence and are completely free from powderiness and opacity which is not the case of previous report by likes of S. M. Rozati et al [18].

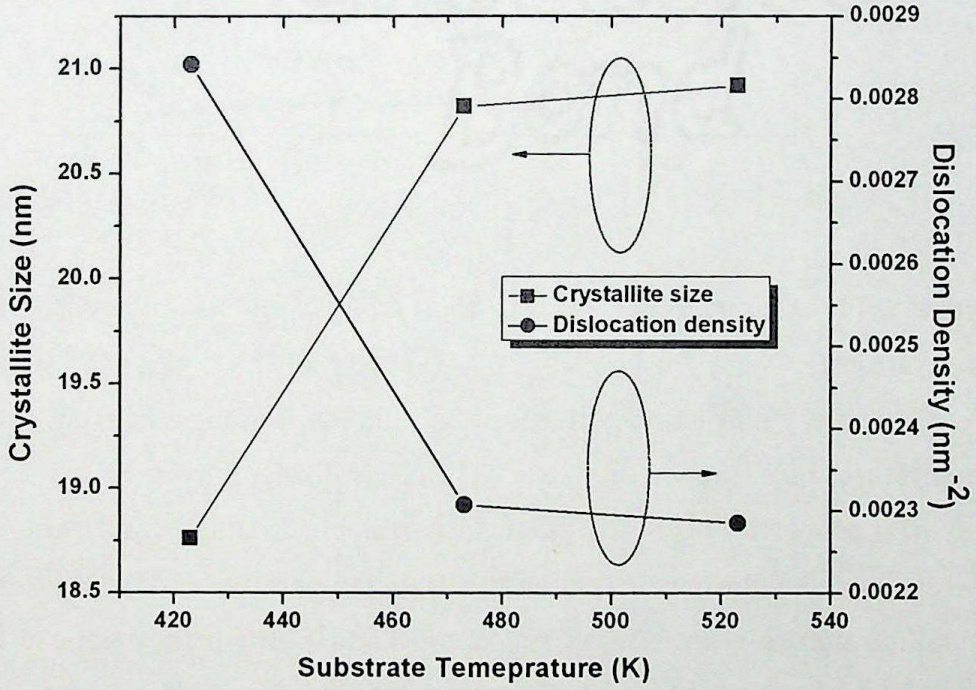


Figure 2.12: *Crystallite size and dislocation density in ZnO thin films as a function of substrate temperature.*

The quantitative improvement in the crystallinity can be well understood from the estimation of the average crystallite size (D) using the renowned Scherrer equation [5] and is found to increase with growth temperature. It is seen that crystallinity increases from ~18 nm to ~21 nm with the increase in the substrate temperature. The increase in crystallite size with substrate temperature is attributed to the increased surface mobility and resultant grain

growth [19]. These calculations hold up the conclusions drawn from the XRD observations. Furthermore the dislocation density (δ) which is length of dislocation lines per unit volume of the crystal was calculated using the simple approach of Williamson and Smallman [6]. The level of crystallization tends to better at high substrate temperatures due to their small δ values which characterize the amount of defects in the film. The larger D and smaller δ values indicate better crystallization of the film. The variation of crystallite size and dislocation density in ZnO thin films as a function of substrate temperature is depicted in figure 2.12. As can be seen in figure, the better crystallization turned out to be at substrate temperatures above 473K in reference to the D and δ values. Nevertheless, there is an insignificant change in their structural properties of the films deposited at 473K and 523K.

2.3. (B) 2. Surface Morphology

To realize the effect of substrate temperature on surface morphology, film thickness and RMS roughness of ZnO films, field emission scanning electron micrograph (FESEM) and atomic force micrograph (AFM) images of films were studied.

2.3. (B) 2.1 Field Emission Scanning Electron Micrograph (FESEM) Study

FESEM studies were carried out for all samples and figures 2.13(a) and (b) show the FESEM micrographs of the ZnO thin films prepared at 423K and 473K substrate temperatures, respectively.

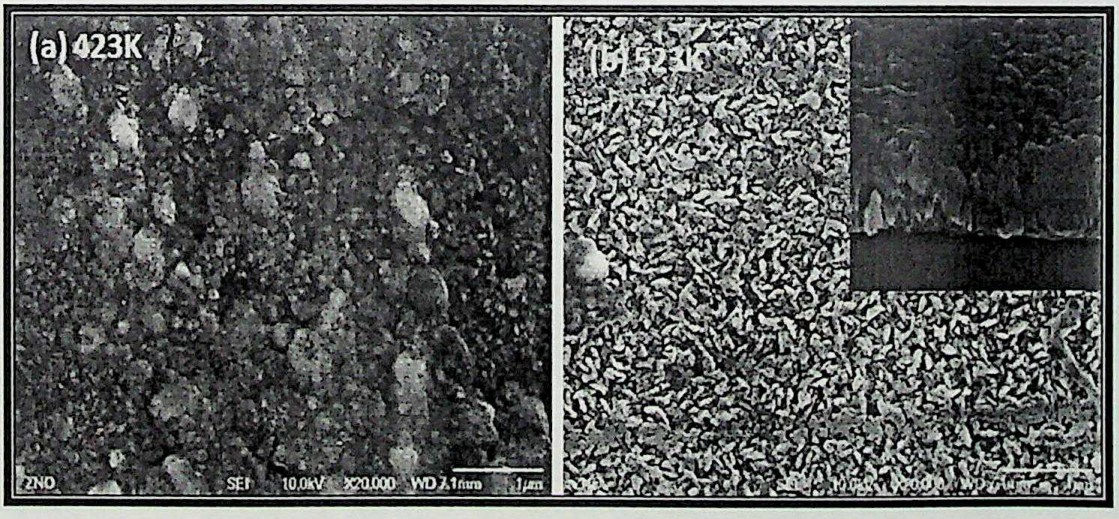


Figure 2.13 *Plain view FESEM micrographs for ZnO films prepared at various Substrate temperatures: (a) 423K, and (b) 523K.*

Both the micrographs show the polycrystalline nature of the film, with a dense surface well covered with the deposits. The surface of the film grown at 423K seems rough and blurred; believably due to the grain growth restricted by insufficient thermal energy. Whereas, the film deposited at 523K possesses a columnar growth as shown by tilted view in the inset of figure 2.13 (b) and consists of uniformly distributed lenticular-like grains. It consists with the better crystal quality at high temperature showed in XRD patterns. The grain size calculated from the XRD studies was found to be smaller than the grain size observed by FESEM. It signifies that these grains may be an aggregation of crystallites.

Moreover, the cross-sectional view FESEM micrographs are obtained to evaluate the film thickness. Typical cross-sectional view FESEM micrograph for ZnO films prepared at 473K substrate temperature is shown in figure 2.14. From the FESEM image, we can notice that the film adheres well with the glass substrate without any pores within the film. Film has a uniform thickness on a microscopic scale. The measured average thickness of film is about 216.5nm. The thickness of the other ZnO thin films prepared at 423K and 523K are found to be ~265 and ~195nm respectively. Thus the ZnO film thickness is influenced by the growth temperature and it decreases with an increase in substrate temperature. The change of film thickness (nm) with substrate temperature is shown in figure 2.15.

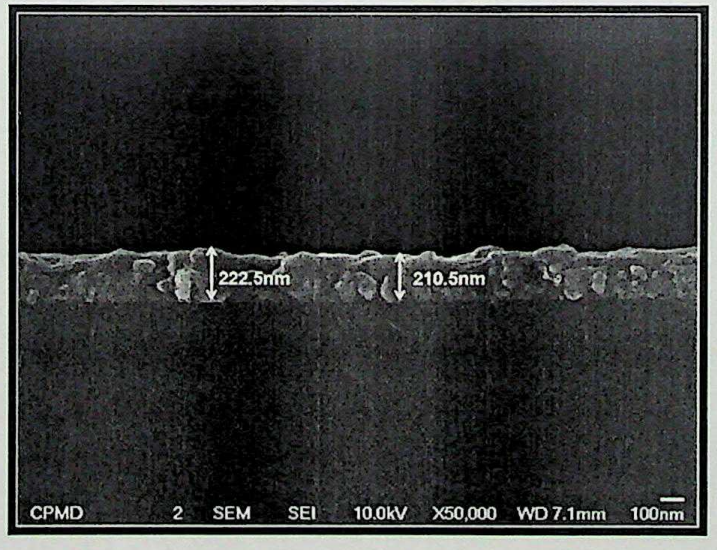


Figure 2.14: *Typical cross-sectional view FESEM micrographs for ZnO films prepared at 473K substrate temperature.*

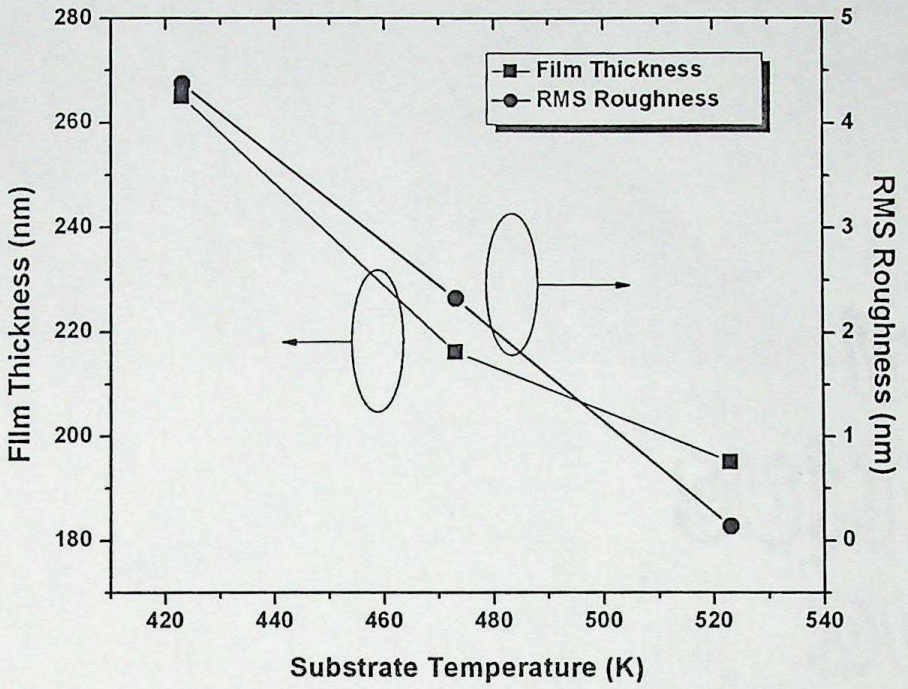


Figure 2.15: *Variation of film thickness (nm) and RMS roughness (nm) with substrate temperature.*

2.3. (B) 2.2 Atomic Force Micrograph (AFM) Study

The AFM images shown in figure 2.16 illustrate the effect of the substrate temperature on the surface morphology of ZnO thin films. As seen in figure, the surface morphology of the ZnO thin films shows an increasingly dense and smooth surface with increase in substrate temperatures. The RMS roughness value decreases with increasing growth temperature and the estimated root-mean-square (RMS) values for the samples grown at temperatures 423K, 473K and 523K are 2.37, 2.31 and 0.13 nm, respectively. This may be ascribed to the fact that the respective grains have increasingly similar growth rates at high temperature, as observed in figure 2.16 (c). The variation of the RMS roughness with substrate temperature is shown in figure 2.15. From figure it is clear that the trend of the variation of RMS roughness is analogous to that of film thickness as a function of substrate temperature.

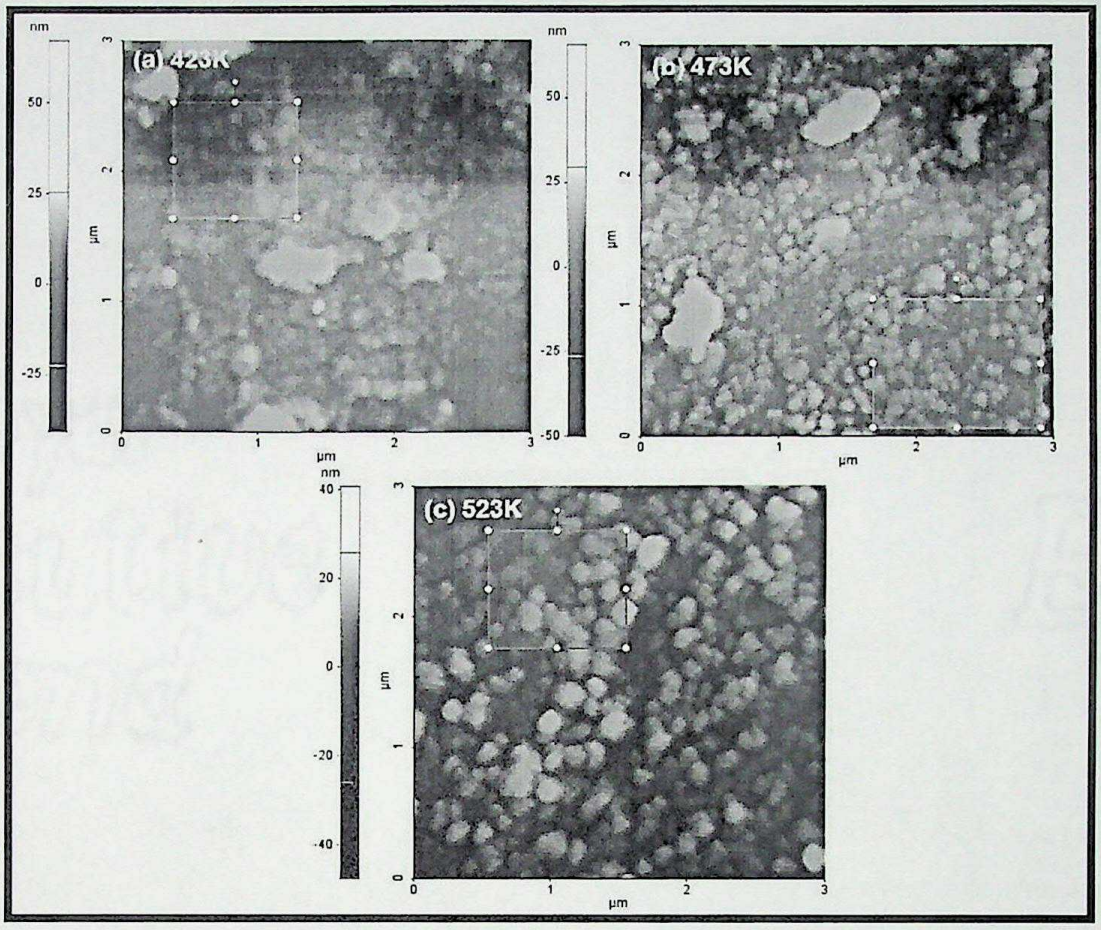


Figure 2.16: *AFM images for ZnO films grown at various substrate temperatures: (a) 423K, (b) 473K and (c) 523K.*

2.3. (B) 3. Electrical Resistivity

The d. c. electrical resistivity (ρ) of the ZnO thin films was measured as a function of temperature in the range 300 to 400 K using two-probe method. Figure 2.17 (a-c) shows the plots of ln (ρ) versus 1000/T for the advanced sprayed ZnO thin film deposited at different substrate temperatures. It is seen that resistivity decreases linearly with increase in temperature indicating semiconducting behavior of zinc oxide. The room temperature electrical resistivity was observed to vary from $\sim 10^{1}\Omega$-cm to $\sim 10^{-1}$ Ω-cm when substrate temperature varies from 423K to 523K with a step of 50K. This electrical resistivity found in the present study was analogous to reported earlier [19]. Interestingly, all plots shows only one slope. Thus it is concluded that as-deposited ZnO film despite of low substrate temperature (i. e. ≤523K) deposition by present spray pyrolysis technique do not show two regions which might be

due to hydroxide and some other impurity inclusions which is a most commonly observed phenomenon.

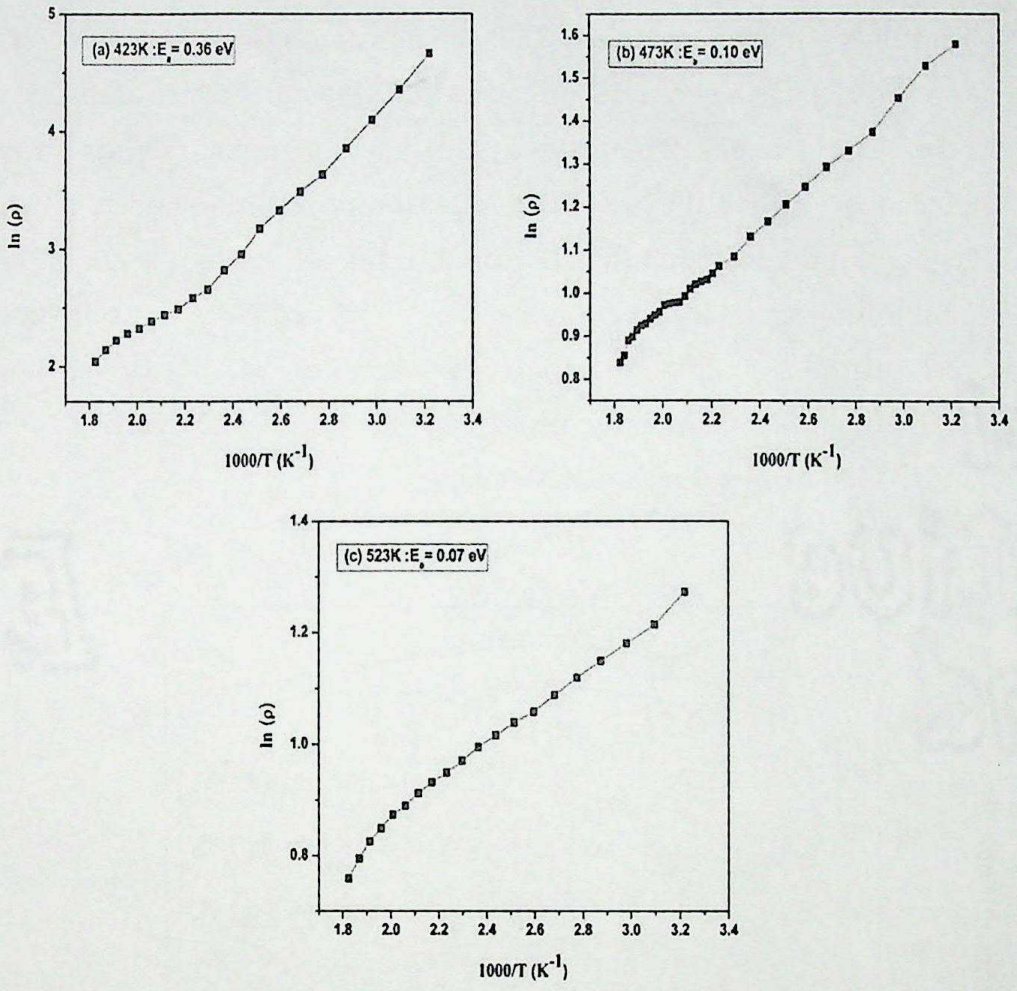


Figure 2.17: *The variation of ln (ρ) with (1000/T) of ZnO thin film grown at various substrate temperatures.*

Moreover, the estimated activation energy values are 0.36eV, 0.10eV and 0.07eV for the films grown at 423K, 473K and 523K respectively.

2.2. (B) 4. Optical Absorption Studies

Figure 2.18 shows the room temperature transmittance spectrum of ZnO thin films grown at different substrate temperatures. The respective variation of optical absorbance of ZnO films with wavelength is shown in inset. The average transmittance of the films including glass substrates in the visible range is over 82% at 550nm. With increasing growth temperature, the transmittance of the films is increased. This variation is mostly determined by the film thickness and

RMS roughness. In the present study, the thickness and RMS roughness of film decreases with increase in substrate temperature. This decrease in the film thickness and roughness decreases the absorption due to the lessening of radiation scattering at the film surface. Thus the film deposited at high substrate temperature (523K) has higher transmittances (~90%) and sharper absorption edge. On the other hand, low temperature (423K) deposited film exhibits lower transmittance (~82%) and the less sharp onset of the absorption edge, this is due to the fact that the scattered radiation became remarkable as a result of the higher film thickness and surface roughness. The influence of substrate temperature particularly at substrate temperature ≥473K on visible transmission of ZnO films is slightly, which may due to the slight variations in crystallite size and RMS roughness of ZnO films.

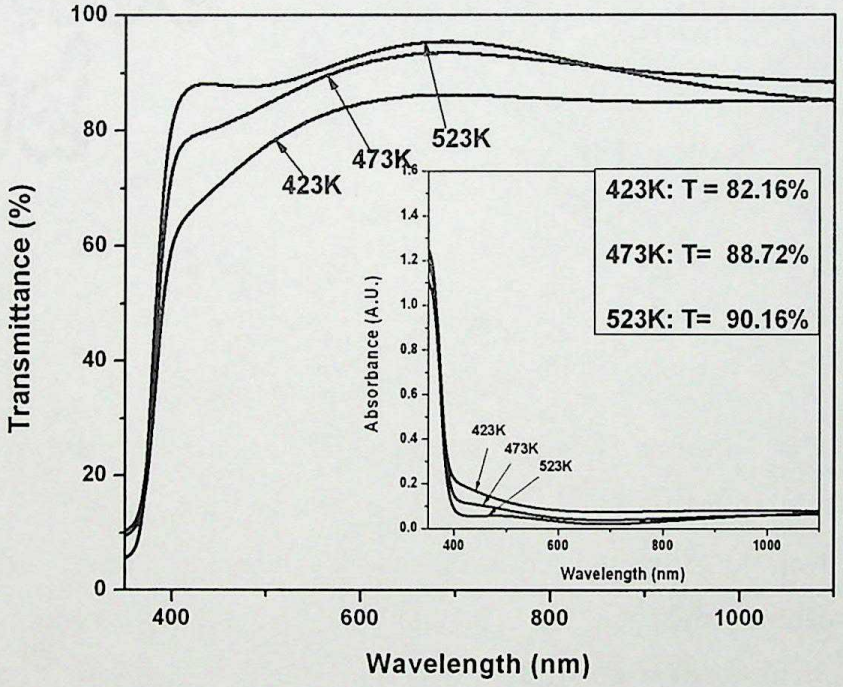


Figure 2.18: *Optical transmission spectra of Zn0 films grown at different substrate temperatures.*

The recorded optical absorption data was further used to evaluate the band gap energy. Figure 2.19 shows the plot of $(\alpha h\upsilon)^2$ vs. $h\upsilon$ for Zn0 films deposited at different substrate temperatures. The band gap is thus determined by extrapolating a linear portion of the plot to the energy axis at $\alpha = 0$. It was

seen from figure that the band gap is slightly decreased from 3.2756eV to 3.2665 eV as the substrate temperature increased from 423K to 523K. The change in band gap may be attributed due to increased crystallinity of the films [15], since the crystallite size improves with the increase in substrate temperature. Such a slight red shift of energy gap appeared with increase of substrate temperature, the trends and the values of energy gap are similar to those reported in the literature [20].

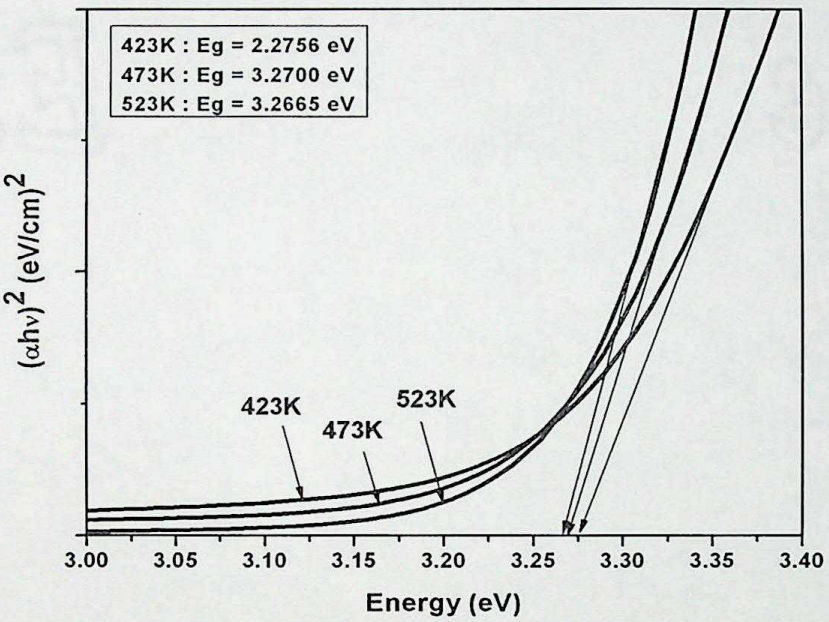


Figure 2.19: *The plot of $(\alpha h\upsilon)^2$ vs. $h\upsilon$ for ZnO films deposited at different substrate temperatures.*

Section (C): Effect of ZnO film thickness

2.3. (C) 1. Surface Morphology

In order to get information regarding the surface morphology, film thickness and RMS roughness of ZnO films, scanning electron micrograph (SEM), field emission scanning electron micrograph (FESEM) and atomic force micrograph (AFM) images were studied.

2.3. (C) 1.1 Scanning Electron Micrograph (SEM) Study

To determine the thickness of the ZnO films deposited at different volumes of spray solution, the cross-sectional view field emission scanning

electron micrographs (FESEM) of the as-deposited ZnO Films were used. Figure 2.20 (a) to (d) shows the cross-sectional view FESEM micrographs for ZnO films prepared by spraying 50, 100, 150 and 200ml spray solution, respectively. It can be seen from the cross-sectional morphologies that the films deposited are compact, and strongly adherent to the substrate. As the volume of spray solution is varied from 50ml to 200ml with a step of 50ml, ZnO film thickness was observed to vary as ~135 nm, ~216 nm, ~298 nm, and~392 nm. The effect of volume of the sprayed solution on ZnO film thickness is shown in figure 2.21.

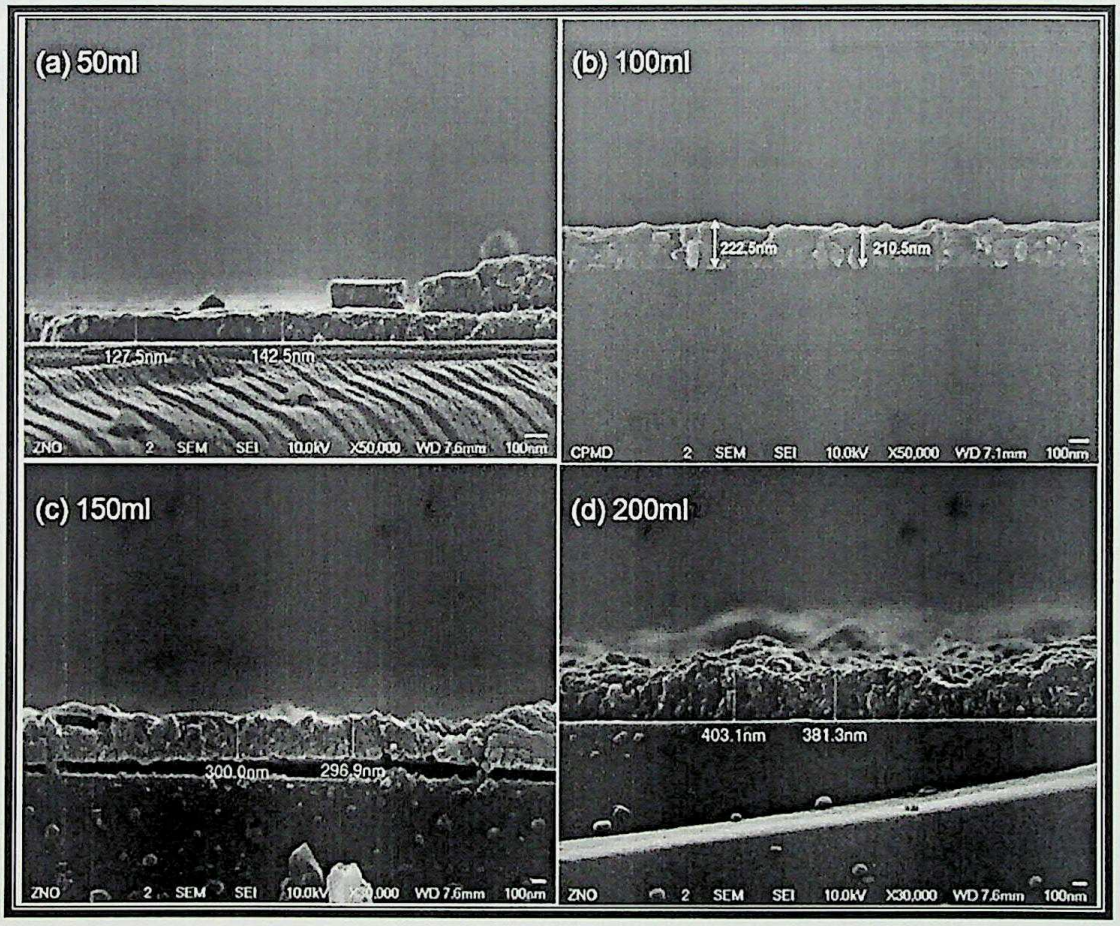


Figure 2.20: *Cross-sectional view FESEM micrographs for ZnO films prepared at different volumes of spray solution: (a) 50ml, (b) 100ml, (c) 150ml and (d) 200ml.*

The in-plane scanning electron micrographs (SEM) of the ZnO thin films with different thicknesses are shown in figure 2.22. All the films are crack-free, constituted by numerous spherical grains, and exhibit the dense and uniform morphology. At 135nm thickness, the film appears smoother; while the surface smoothness appears to reduce with an increase in film thickness. It is also observed that the grain size increases when the thickness increases.

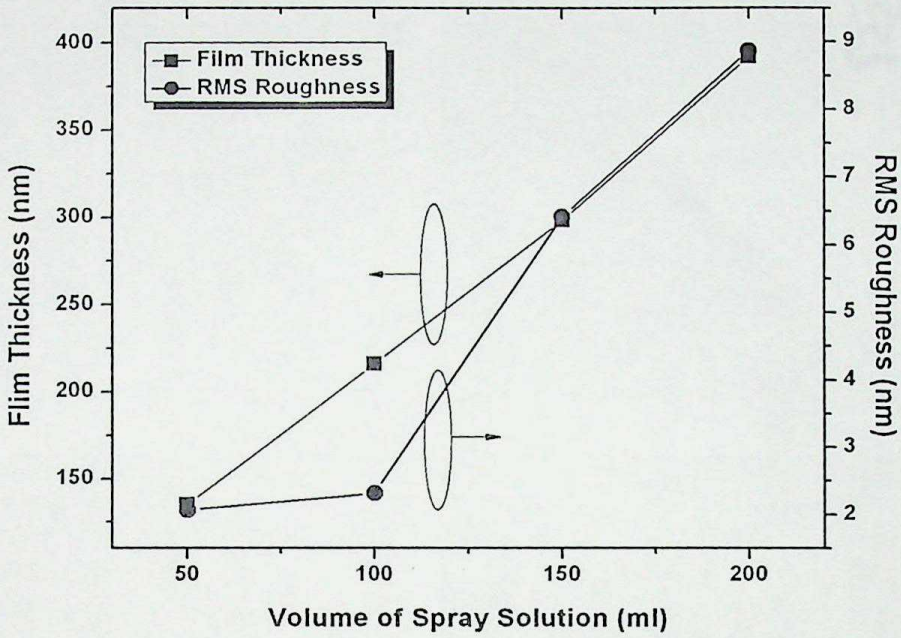


Figure 2.21: *Variation of film thickness (nm) and RMS roughness (nm) with volume of spray solution (ml).*

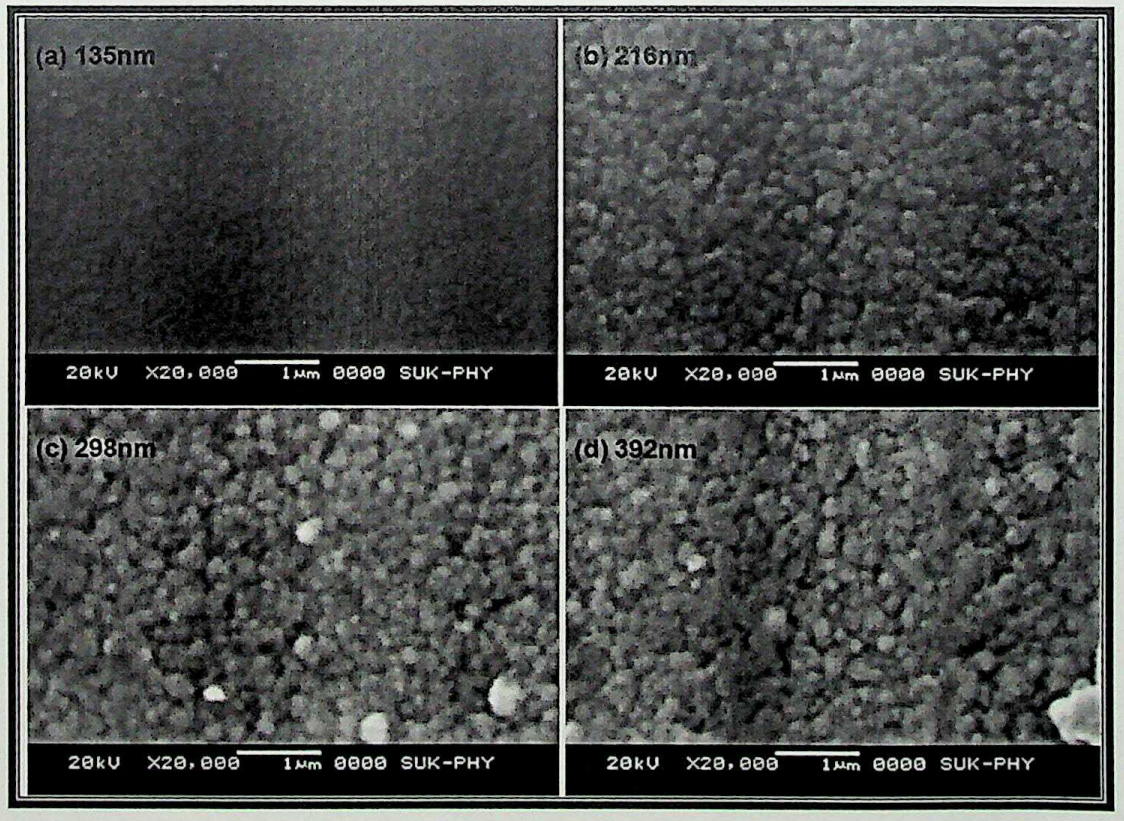


Figure 2.22: *SEM micrographs of ZnO thin films of thickness (a) 1356nm, (b)216nm, (c)298nm and (d) 392nm.*

2.3. (C) 1.2 Atomic Force Micrograph (AFM) Study

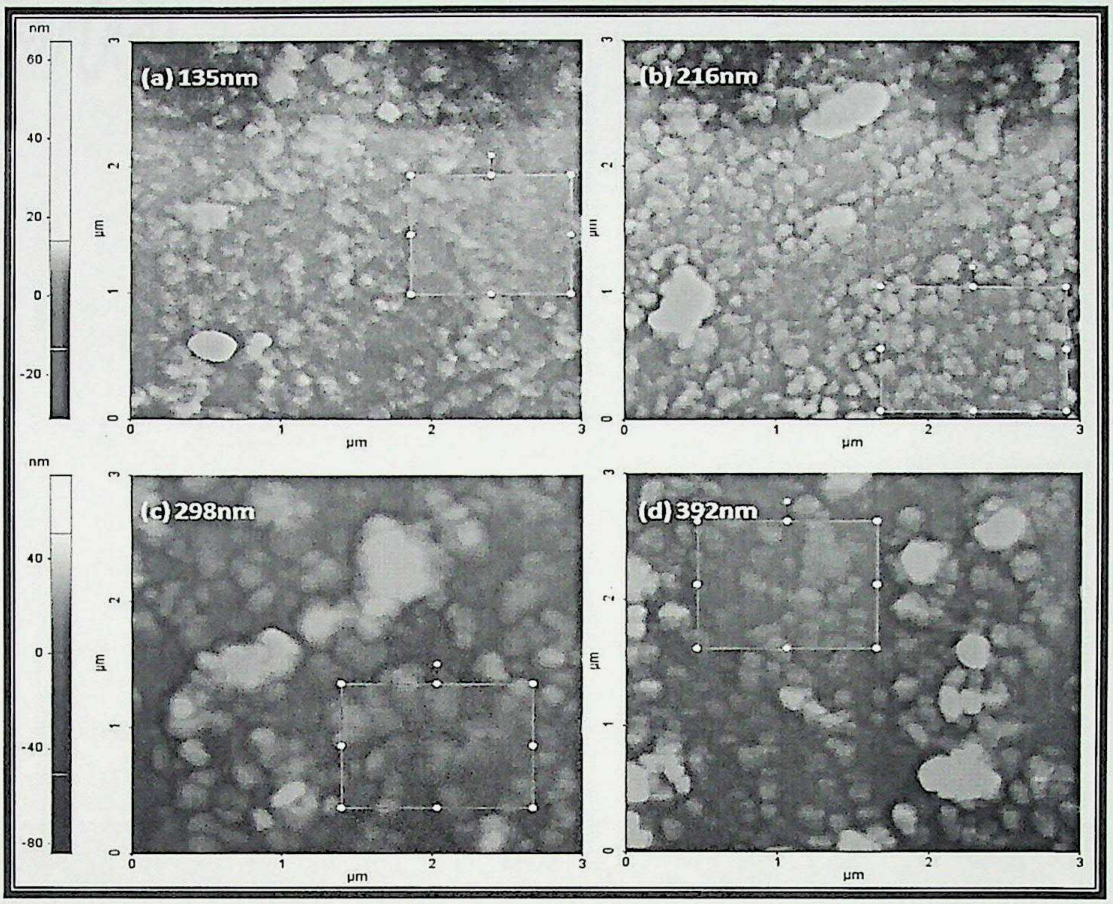


Figure 2.23: *AFM images of ZnO thin films of thickness (a) 135nm, (b)216nm, (c)298nm and (d) 392nm.*

Atomic force microscopy was used as well in order to support the observations of the ZnO films made from the SEM images. Figure 2.23: (a)-(d) shows the AFM images of the surface of ZnO films of different thicknesses (135-392 nm). Figure depicts well covered surfaces with spherical shape grains and with increase in the thickness of the film the grains grew in size. The surface root mean square RMS roughness were estimated from the images and found to be increasing with increasing thickness (Figure 2.21). The surface roughness for 135nm was found to be minimum (~2.0nm) due to homogenous distribution of crystallites. The surface roughness increased to ~8.9 nm with further increasing thickness of film to 392 nm. The increase of RMS roughness with film thickness may be attributed to the development of the larger grains by agglomeration of smaller grains. Thus, the dependencies amongst roughness and thickness pursue a linear law. Similar linear relationship between thickness and RMS roughness

was observed by M. Suchea et al for pulsed laser deposited ZnO thin films [21].These results suggest that the film thickness control can definitely be realized through varying the volume of sprayed solution.

2.3. (C) 2. X-ray Diffraction Studies

Figure 2.24 shows XRD patterns of advanced spray pyrolysis derived ZnO thin films with different thicknesses. For film with 135 nm thickness, apparent hump around 20 to 33° indicates amorphous mixed nanocrystalline phase of deposits. Similar hump was observed by S. S. Shinde et al for the sprayed fluorine doped zinc oxide thin films [22]. The Swelling background may be due to interactions of the X-rays with the underlying amorphous substrate material. For higher thicknesses, the matching of observed and standard d-values revealed (100), (101), (102) peaks with a preferential oriented (002) peak. The position of the measured diffraction peaks and the growth orientations are independent of the film thickness. But the intensities of the peaks, especially the (002) peak increases with increasing the film thickness. Such structural changes in respect to the thickness can be understood easily; in case of samples with sufficient thickness there is enough material which can diffract the incident X-rays and thus results in more intense peak. Whereas the relatively thinner samples undergo less diffraction and the noise in the measured spectra is so significant that it hides any form of growth orientation. This signifies that the improvement in crystallinity with increase in film thickness. The similar results were also reported by others [23, 24]. This suggests that ZnO films prepared by advanced spray pyrolysis are polycrystalline ZnO with hexagonal (wurtzite) crystal structure and show a preferential orientation along c-axis Perpendicular to the substrate. The c-axis orientation in ZnO films can be realized by the Drift's "survival of the fastest growing crystallites" model [25]. In accordance with this model, nucleations with various orientations can be formed at the preliminary stage of the deposition and each nucleus competes to grow up; however only nuclei having the highest growth rate can survive, i.e., c-axis orientation is achieved.

The average crystallite size of the ZnO thin films of different thicknesses has been calculated using Debye-Scherrer's formula [5]. These values are shown in figure 2.25. From figure it is seen that the thickness effect upon the crystallite

size comes into view mainly in the thinnest films, the thickness of which is lower than approximately 298nm. In this range the crystallinity is intimately interrelated to the film thickness. But a trend of saturation or slight reduction in crystallite size versus film thickness was observed beyond that range. Similar behavior of the crystallite size in ZnO thin films as a function of film thickness is observed by M. Bouderbala et al [24]. In addition, to get more information on the amount of defects in the films the dislocation density was calculated using the formula $\delta = \frac{1}{D^2}$ [6]. The δ values are shown in figure 2.25. The increasing crystallite sizes (D) and decreasing dislocation densities (δ) imply the better crystallization of the films with increase in thicknesses.

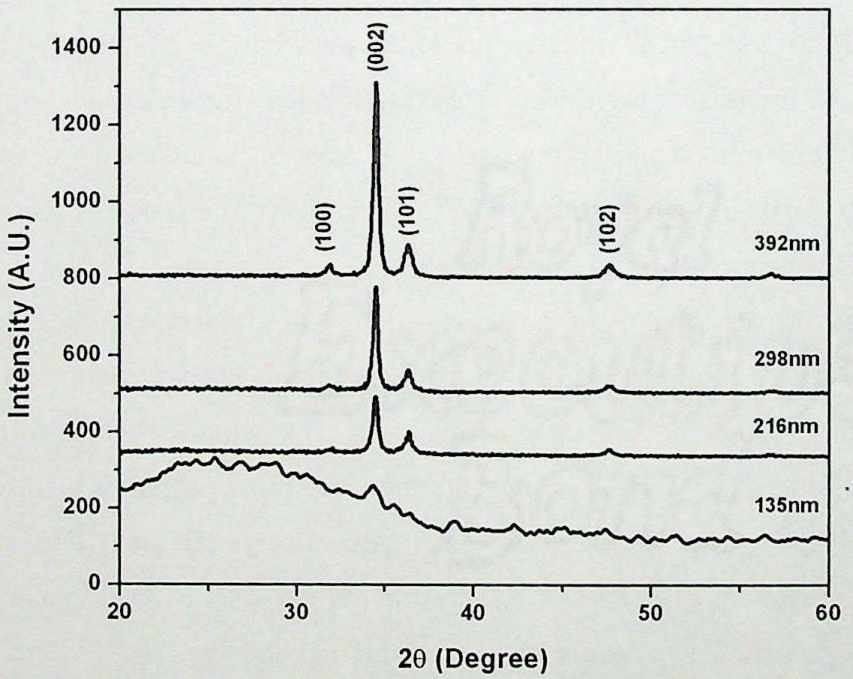


Figure 2.24: *XRD patterns of ZnO thin films with different film thickness.*

Furthermore, the lattice constants 'a' and 'c' of the wurtzite ZnO were calculated using the equation [26],

$$d_{hkl} = \left(\frac{4}{3} \frac{h^2 + hk + k^2}{a^2} + \frac{l^2}{c^2} \right)^{-1/2} \quad \text{---------- (2.9)}$$

The observed 'c' and 'a' values are 5.210Å and 3.243Å respectively and are in good agreement with the standard values taken from the Joint Committee of Powder Diffraction Standards (JCPDS) card 05-0662.

Additionally, the Zn-O bond length 'L' is estimated by [27],

$$L = \sqrt{\left[\frac{a^2}{3} + \left(\frac{1}{2} - u\right)^2 c^2\right]} \quad \text{---------- (2.10)}$$

Where the parameter 'u' in the wurtzite crystal structure is specified by,

$$u = \frac{a^2}{3c^2} + 0.25 \quad \text{---------- (2.11)}$$

Herein, it is related to the c/a ratio which is 1.6065. The estimated Zn-O bond length is 1.9754Å.

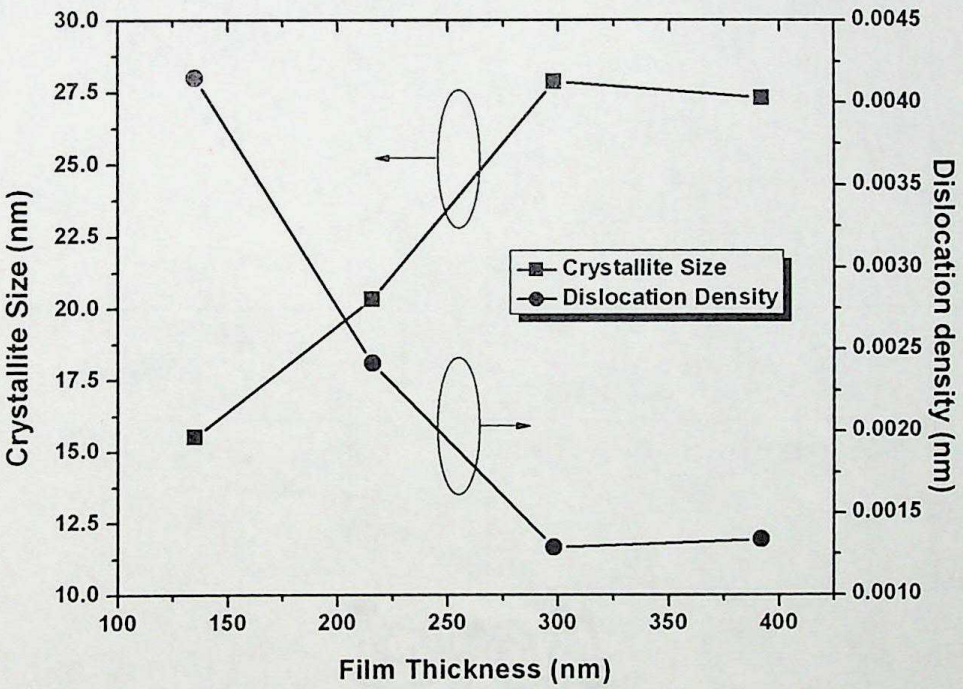


Figure 2.25: *Crystallite size and dislocation density in ZnO thin films as a function of film thickness.*

2.3. (C) 3. Electrical Resistivity

The variation of log ρ with reciprocal temperature (1/K); of ZnO films with various thicknesses are depicted in figure 2.26. In case of the ZnO film of 135 nm thickness, the resistivity plot is approximately horizontal in the range 3.2 (K^{-1}) to 2.3 (K^{-1}) and tends to become linear in the range 2.3 (K^{-1}) to 1.8 (K^{-1}).

This behavior can be explained as follow: In case of this sample, the lowest crystallite/grain size causes the largest grain boundary density to be profoundly involved in the oxygen molecule chemisorption process. Due to this the 135 nm sample has the largest resistivity amongst all. Further, it seems that in the virgin state of the film these molecules have an empirical binding energy of about 0.037eV (~435 K) which is supplied to the sample in heating cycle in the resistivity measurement, when the molecule starts to leave the sample rapidly and the conductivity increases, this can be observed in the plot. For the other samples the plot is almost linear.

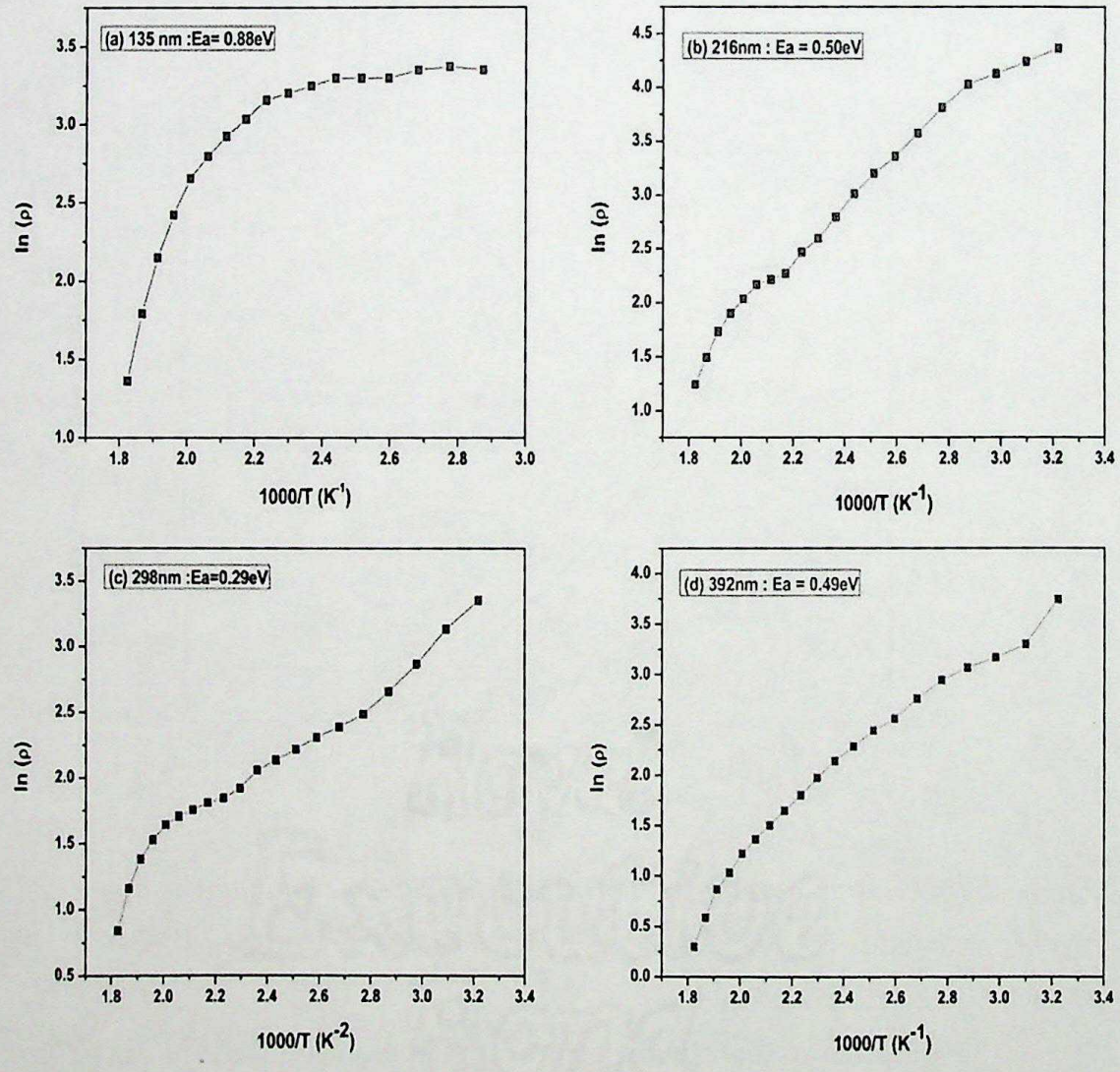


Figure 2.26: *Electrical resistivity of zinc oxide thin films onto glass substrate with reciprocal of temperature (1000/T) for various film thicknesses: (a) 135nm (b) 216nm (c) 298nm and (d) 392nm.*

The room temperature electrical resistivity of as-deposited ZnO film was of the order of 10^1 Ω-cm which decreased with temperature indicating the normal semiconductor behavior. On the other hand, the room temperature resistivity of ZnO film was decreased from >21Ω-cm to 1M Ω-cm with increase in film thickness from 135nm to 392nm. Thus the room temperature resistivity of sprayed ZnO films falling almost linearly with increasing thickness, in which the decreasing trend can be attributed to the inverse linear dependence of film resistivity increase on grain size [28]. The growth in grains with film thickness leads to reductions in grain boundary scattering due to charge carriers, thus decreases the resistivity for the obtained films and eventually reduces the film resistivity. Similar resistivity behavior was observed by M. Bouderbala et al [24] and M. Suchea et al [21].

Further, the activation energies were calculated by applying the resistivity equation (2.7). Activation energy (E_a) was calculated from the slope of ln (ρ) versus 1/T curve [29]. The activation energy for ZnO films with 135, 216, 298 and 392nm thickness was found to be 0.88, 0.50, 0.29 and 0.49eV respectively.

2.3 (C) 4. Optical Absorption Studies

Optical characterization of thin films gives information about other physical properties, e.g. band gap energy and band structure and optically active defects etc. The effect of thickness on the optical transmittance and the band gap (E_g) values of the ZnO films have been studied. Figure 2.27 shows the transmittance spectrum as a function of the wavelength for the ZnO films with different thickness; the inset shows the optical absorption spectrum vs. wavelength. At 550nm, the average transmittance of the films including substrates in over 80%. The transmission decreases sharply near low wavelength region due to the band gap absorption. With increasing film thickness, the transmittance of the films is decreased due to the thickness and roughness effect. With increasing film thickness, the increase in roughness increases the surface scattering effect and hence results in the reduction in the transmittance. This effect was anticipated as increasingly photons are adsorbed in a material when the thickness is increased. Additionally, a shift of the absorption edge proportional to the thickness values, towards UV energies is

evident from the spectra. This blue shift of absorption edge may be ascribed to the difference in grain size [30].

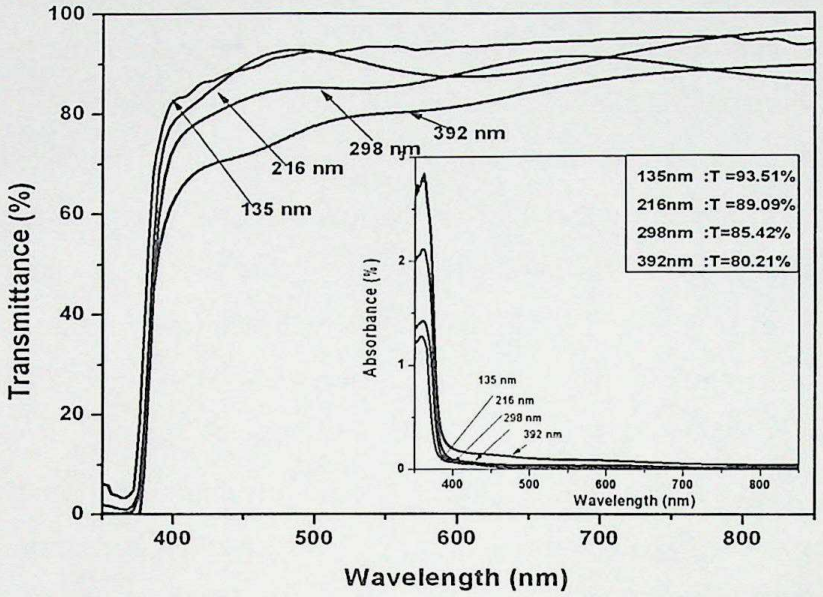


Figure 2.27: *Optical transmittance spectra versus wavelength for ZnO thin films with different thickness: 135 nm, 216 nm, 298 nm, 392 nm.*

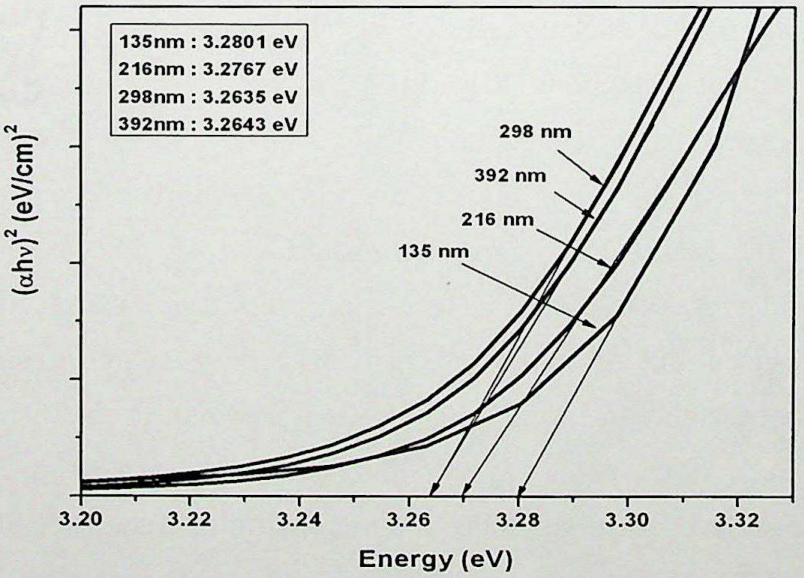


Figure 2.28: *Variations of (αhυ) ² versus hυ for ZnO thin films with different film thickness.*

Furthermore, to determine the optical band gap 'E_g' of as prepared ZnO films the Tauc's plot [13] i. e. $(\alpha h\upsilon)^2$ vs. $h\upsilon$ is plotted in figure 2.28. The energy band gap is then determined from the intercept of extrapolated linear part of the curve with the energy axis. The optical energy band gap of the films decreased from ~3.28eV to ~3.27eV as the thickness increased from 135nm to 298nm. Further, a very minor blue shift of 0.0008eV was observed when thickness is changed from 298nm to 392nm. The resultant values of E_g have been given in figure 2.28. Thus the film thickness has a significant effect on the optical energy band gap. As can be seen from the XRD studies the crystallite size was increased with increasing film thickness up to 298nm; and the band gap exhibits a 'red shift' with an increasing film thickness. For further increase of thickness up to 292nm, the saturation or the slight decrease of crystallite size resulted into the minor blue shift. Therefore, the both shifts of band gap energy of ZnO thin films with increasing film thickness are accredited to the quantum size effect. A similar optical band gap shift was observed by others [31, 32].

Section (D): Effect of Layer by Layer [LBL] Deposition

2.2. (D) 1. X-ray Diffraction studies

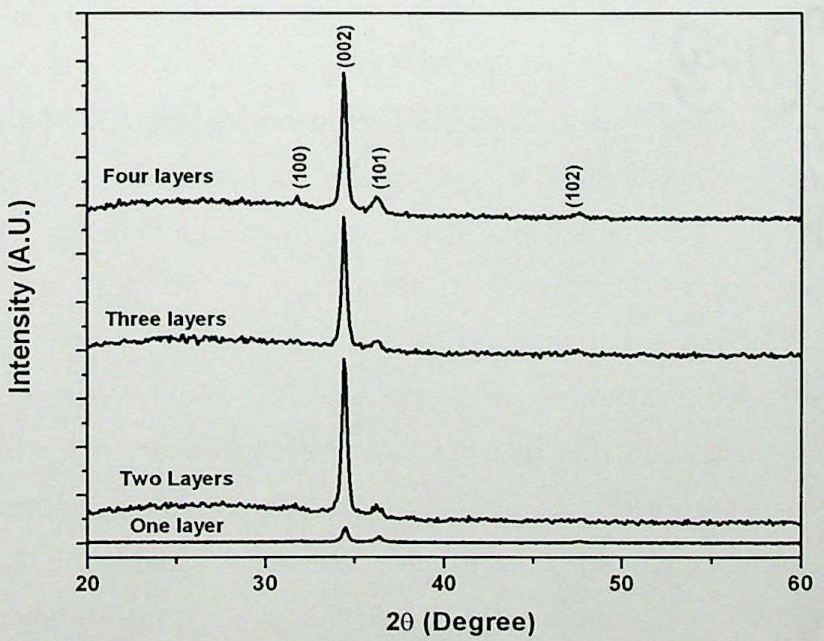


Figure 2.29: *XRD patterns of different number of ZnO thin film layers.*

Figure 2.29 shows XRD patterns of different number of ZnO thin film layers deposited on glass substrates. All the diffraction peaks in the patterns correspond to the reflection of wurtzite-structured ZnO planes and all the samples have a strong (002) peak. This suggests that all the prepared ZnO thin film layers have a hexagonal wurtzite structure and are preferentially oriented along the c-axis perpendicular to the substrate surface. As for monolayer sample, besides the (002) peak, it still has two other peaks, namely (101) peak and (102) peak. However, two and three layer samples exhibit (101) peak along with the (002) peak and the four layer sample exhibits three other peaks namely, (100), (101) and (102) in addition to the (002) peak. With the increase of number of layers, the intensity of (002) peak is increased. The (002) peak position for the monolayer ZnO sample is at 32.5°; while for the double layer sample onwards the peak position is slightly shifted to 32.4°. This may be understood as follows: for the ZnO monolayer the amorphous glass is used as the substrate whereas this monolayer itself used as a substrate for depositing the second layer to for the double layer structure. Thus, there stays the difference between the thermal expansion coefficients between the ZnO film and the substrate onto which it is grown. This fact may leads to the observed lower angle shift of (002) diffraction peak by 0.1°. However, in case of three and four layer samples, for the upper layer the substrate used remains the same as ZnO film; so there is not further shift observed for (002) peak.

The average crystallite size has been estimated from the full width at half maximum (FWHM) of the (0 0 2) peak using the Scherrer formula [5]. These values are illustrated in figure 2.30. Similar to the behavior of the crystallite size with thickness variation observed in section (c), in the present study the crystallite size increases with the increase of number of ZnO layers and the three layer sample exhibits a largest crystallite size of ~26nm. While a trend of saturation or slight reduction in crystallite size was observed for four layer sample. Besides, the dislocation density was estimated using the approach of Williamson and Smallman [6]. The δ values are also illustrated in the same figure 2.30. The highest crystallite size (D) with smallest amount dislocation densities (δ) for three layer sample mean the highest crystallization for this sample.

Therefore, comparing the layer by layer deposited structures with the previously studied ZnO film thickness effect, both of them have approximately similar effect on the crystallographic properties.

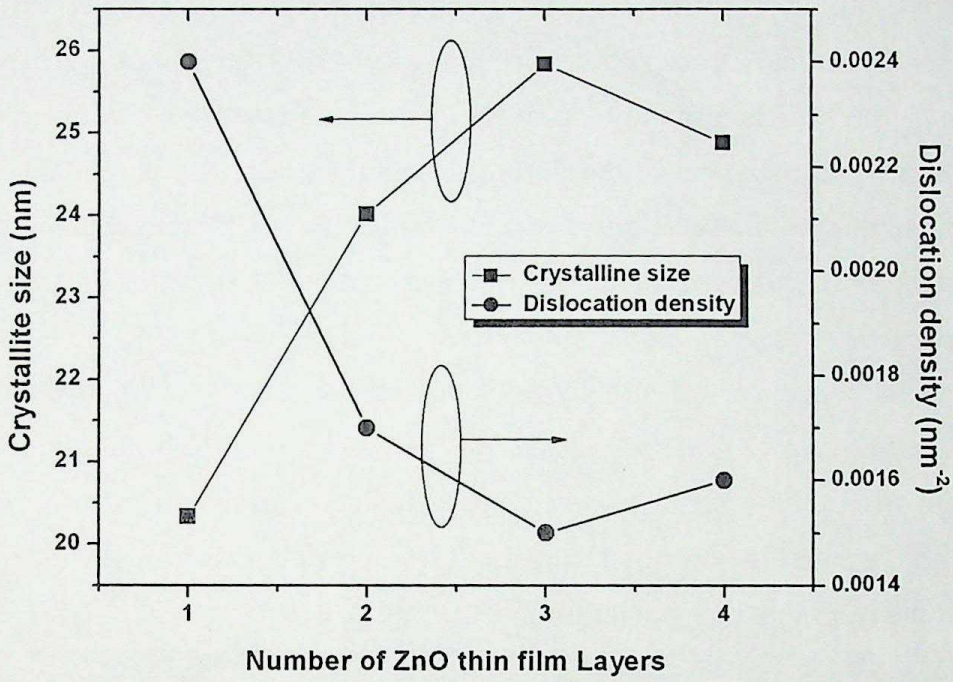


Figure 2.30: *Crystallite size and dislocation density in ZnO thin films as a function of number of ZnO layers.*

2.2. (D) 2. Surface Morphology

To observe the changes in the surface morphology, film thickness, RMS roughness of the ZnO thin film samples with the variation in number of layers, their images obtained with field emission scanning electron microscopy (AFM) and atomic force microscopy are used.

2.2. (D) 2.1 Field Emission Scanning Electron Micrograph (FESEM) Study

Figure 2.31 shows the top view FESEM micrographs of samples with different number of ZnO layers. All the films are crack free, highly dense and well covered with the irregular sized grains. The grain size is observed to be increasing with the increasing number of ZnO layers and this observation well agrees with the calculations made in XRD characterization.

Further, it is noteworthy that some hexagonal shaped grains can be observed on the surface of the double layer film; one of them is shown in the

inset. With further for three layer sample such hexagonal shapes appears most [see inset of figure 2.31 (b) and (c)]; however no any hexagonal shape is appeared for the four layer sample. This is somewhat different as compared to the thickness effect observed in FESEM micrographs for the ZnO film surfaces in section (c). As discussed earlier, in thickness variation case the substrate onto which ZnO film deposited is amorphous glass. Thus the initial nucleation sites are simply provided by this preheated glass substrate for all samples. So even after the improvement in the film thickness the grains are originated from the similar nucleation sites; and hence appear spherical shaped. Whereas in LBL deposition, though the monolayer film uses the nucleation sites provided by the preheated substrate, this highly c-oriented polycrystalline ZnO films forms the basis for further layers and provides different nucleation sites, probably the c-oriented hexagons. Thus, the three layer sample shows a clear hexagonal shaped grain over the surface. However, no such shapes are seen for the four layer sample, may be, due to the saturation of the crystallite size as observed by XRD and the consequent agglomeration of the grains.

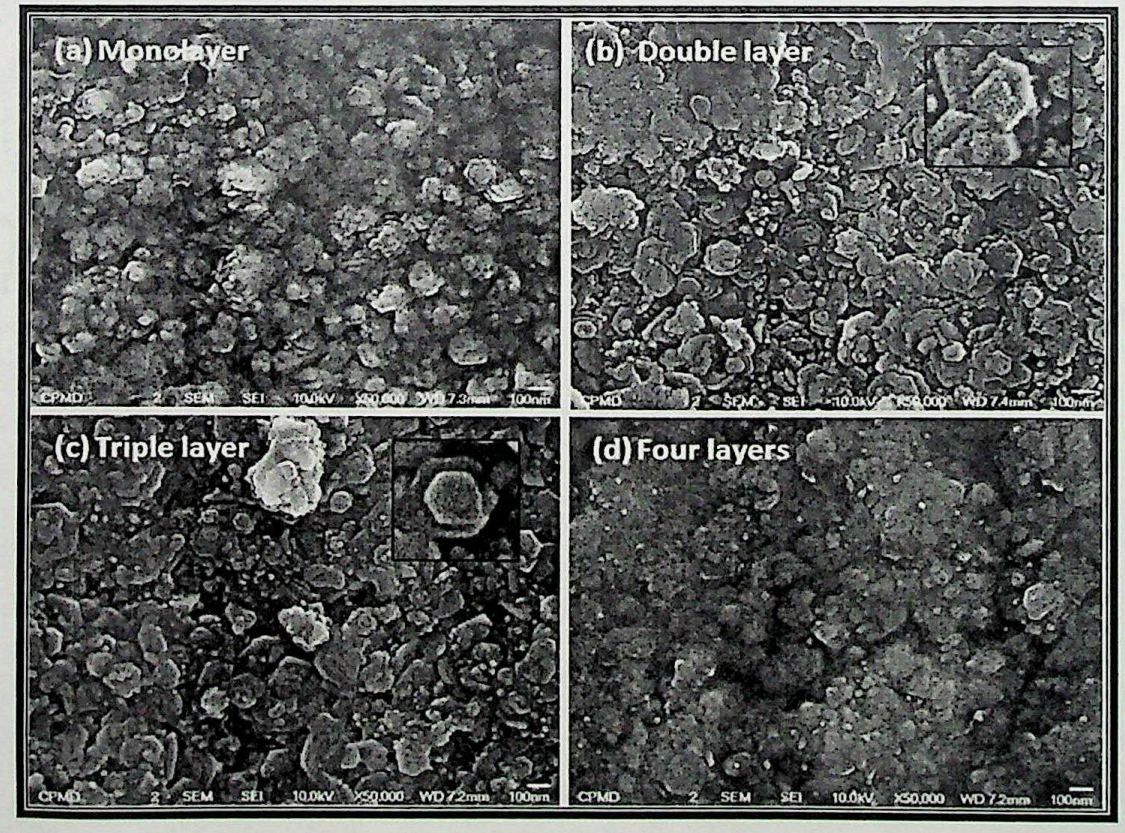


Figure 2.31: *FESEM micrographs of (a) Monolayer, (b)Double layer, (c) Three layer and (d) Four layer ZnO thin films.*

Figure 2.32 (a) to (c) shows the cross-sectional view FESEM micrographs for samples prepared by depositing single, two and four ZnO thin film layers. It can be seen from the cross-sectional morphologies that the films deposited are compact, and strongly adherent to the substrate. Further, the film cross sectional micrographs does not show clear boundaries in between layers; suggests columnar growth of the films. As the number of layers is varied like single, two, three and four by spraying 100 ml spray solution for a single layer, the ZnO film thickness was observed to vary as ~216 nm, ~337 nm, ~465 nm, and ~585 nm. The effect of number of layers on ZnO film thickness is shown in figure 2.33.

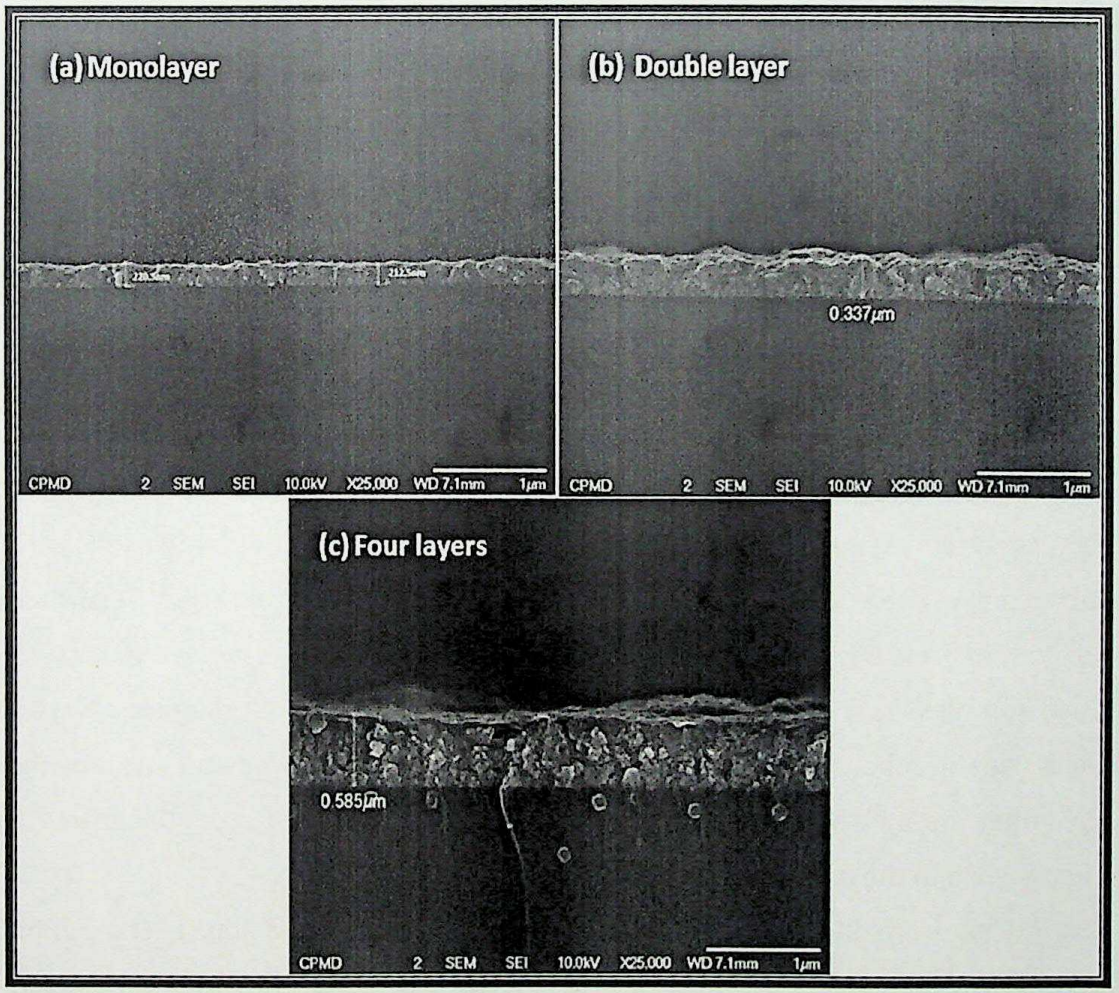


Figure 2.32: *Cross-sectional view FESEM micrographs for different LBL deposited ZnO samples: (a) one layer, (b) double layer and (c) Four layers.*

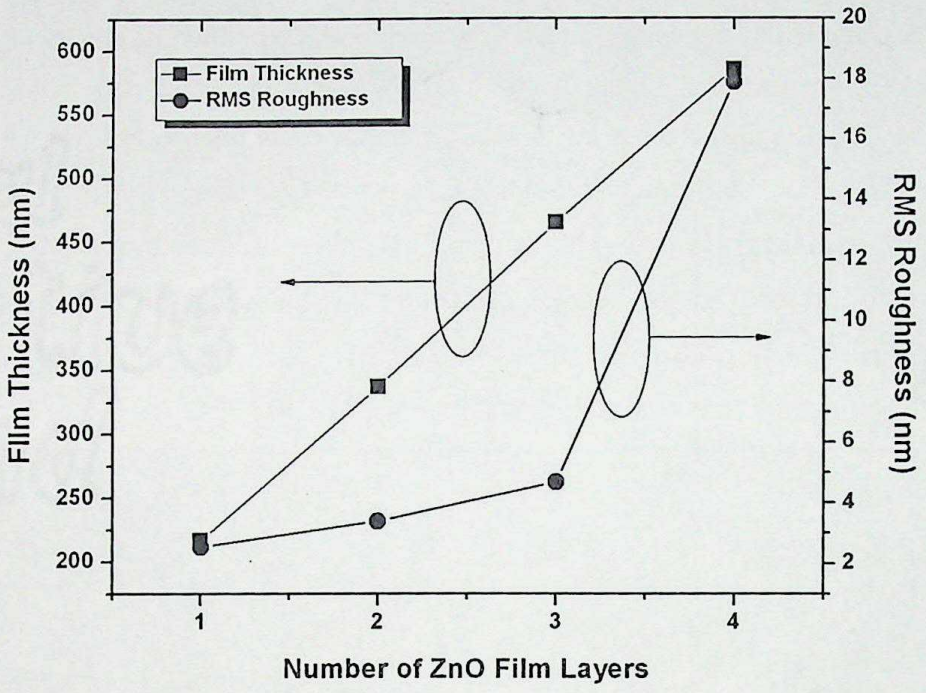


Figure 2.33: *Variation of film thickness (nm) and RMS roughness (nm) with different number of ZnO thin film layers.*

2.2. (D) 2.2 Atomic Force Micrograph (AFM) Study

Figure 2.34 shows the AFM images of the films. The surface roughness factors were estimated from the images and found to be increasing with increasing number of ZnO thin film layers. The root mean square (RMS) surface roughness are 2.54, 3.39, 2.68, and 17.88 nm for single, two, three and four layer ZnO samples respectively (figure 2.33). The increase of roughness with increasing number of ZnO layers is due to increasing thickness and subsequent the larger grain formation and agglomeration. The agglomeration of the grains is clearly seen in the AFM image for the four layer sample.

Therefore, though the LBL deposited samples exhibited similar crystalline properties, the surface morphology for both these cases differs appreciably. However, the thickness variation and RMS roughness values follows the similar trend.

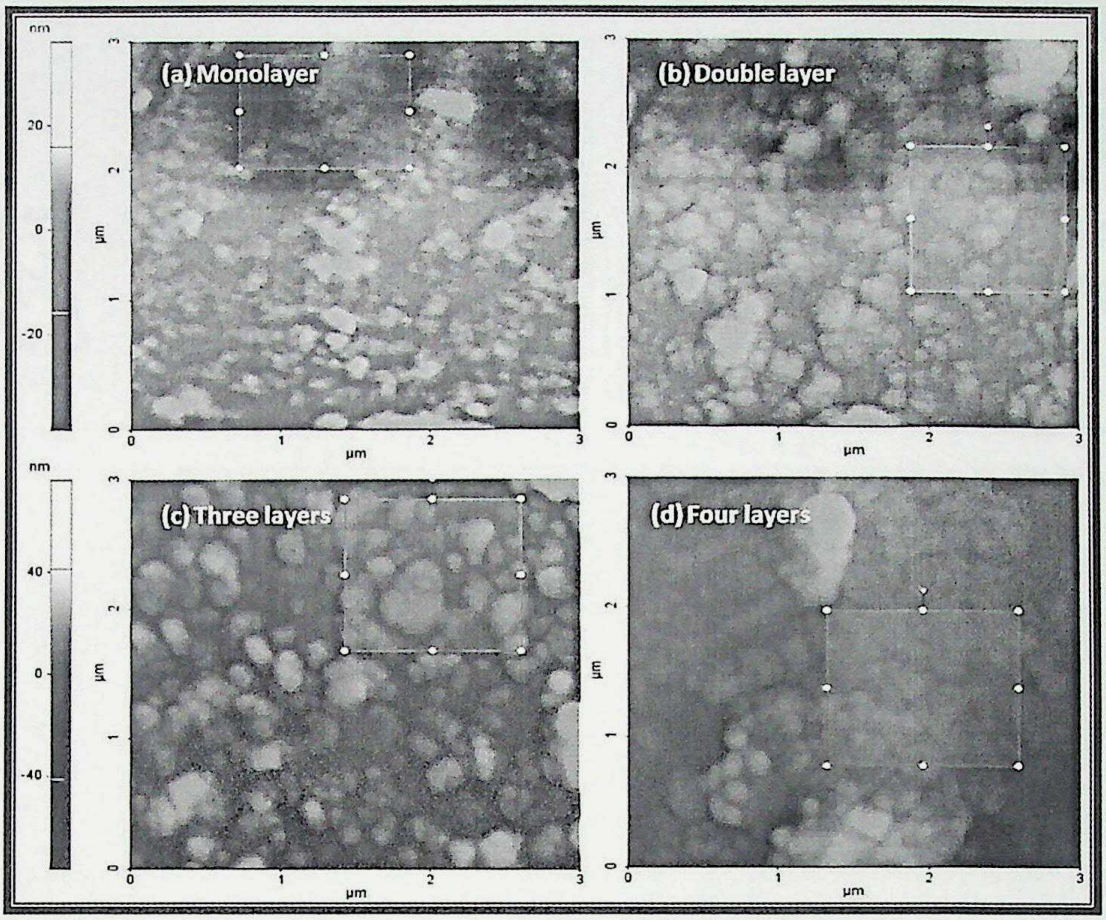


Figure 2.34: *AFM images for different LBL deposited ZnO samples: (a) one layer, (b) double layer and (c) three layers and (d) four layers.*

2.2. (D) 3. Electrical Resistivity

The d. c. electrical resistivity of the ZnO thin films was measured as a function of temperature in the range 300 to 600 K using two-probe method. Figure 2.35 (a)-(d) shows the variation of the electrical resistivity with temperature for the LBL deposited ZnO samples with one layer, double layer three layers and four layers respectively.

It is seen that for all samples resistivity decreases linearly with increase in temperature indicating semiconducting behavior of ZnO. The room temperature electrical resistivity was observed to be of the order of 10^1 Ω-cm. Further, the estimated activation energies for ZnO films with one, two, three and four layers was found to be 0.50, 0.48, 0.31 and 0.40eV respectively. Thus, the LBL deposited ZnO samples possess electrical properties approximately similar to that of thickness varied ZnO thin film samples seen in section (c).

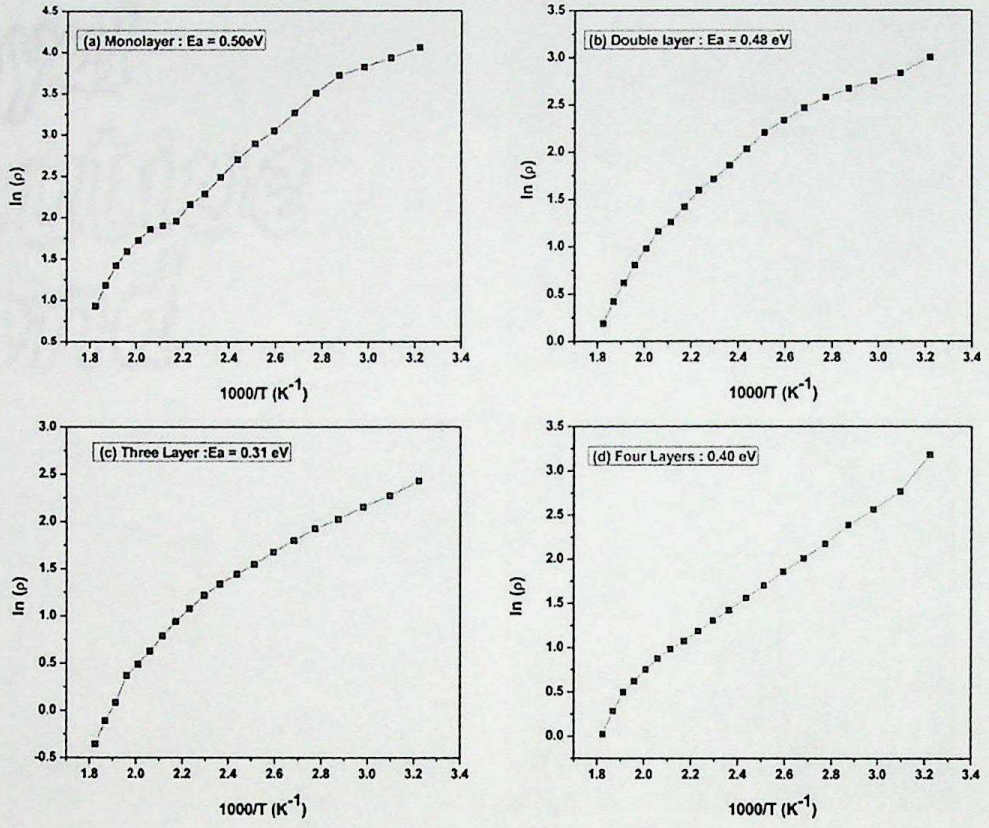


Figure 2.35: *Electrical resistivity with reciprocal of temperature (1000/T) for different LBL deposited ZnO samples: (a) one layer, (b) double layer, (c) three layers and (d) four layers.*

2.2. (D) 4. Optical Absorption Studies

Figure 2.36 shows optical transmittance spectra of ZnO thin film samples with different number of layers. It was observed that the average transmittance decreased from ~89% to 72% in the visible region at 550nm with increase in number of layers. The decrease is attributed to the increased film thickness and RMS roughness. Further, the band gap of the films was determined from the Tauc plots [13] of $(\alpha h\nu)^2$ vs. photon energy. Figure 2.37 shows the $(\alpha h\nu)^2$ vs. photon energy curves of ZnO film samples with varying number of layers. The observed band gap values are given in the inset of the figure. Figure shows the decrease of optical band gap (E_g) towards higher wavelengths for samples with layers varying from one to three, thereafter very small shift towards lower wavelengths is observed for the four layer sample. The band gap behavior is attributed to the quantum size effect associated with the crystallite size estimated in the XRD studies.

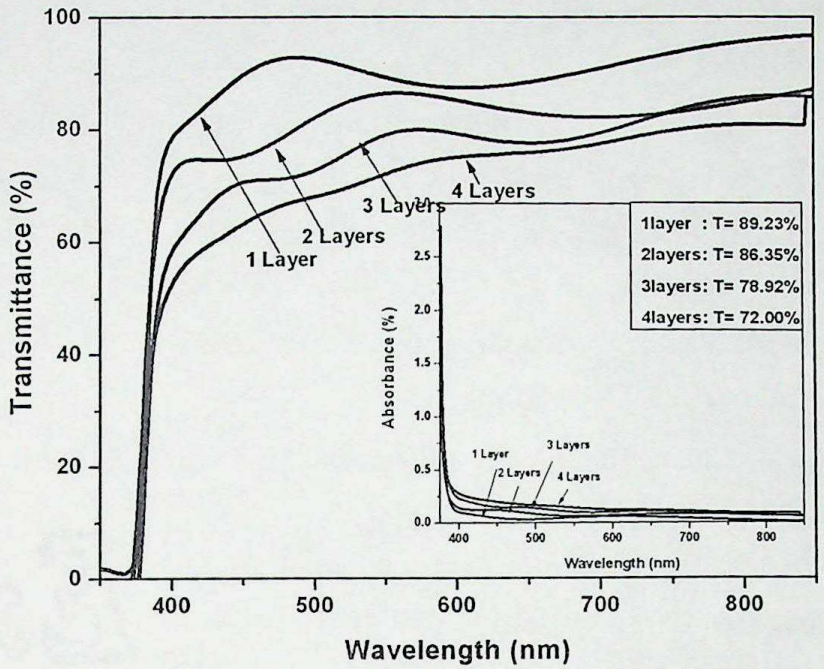


Figure 2.36: *Optical transmission spectra of ZnO thin film samples with different number of layers.*

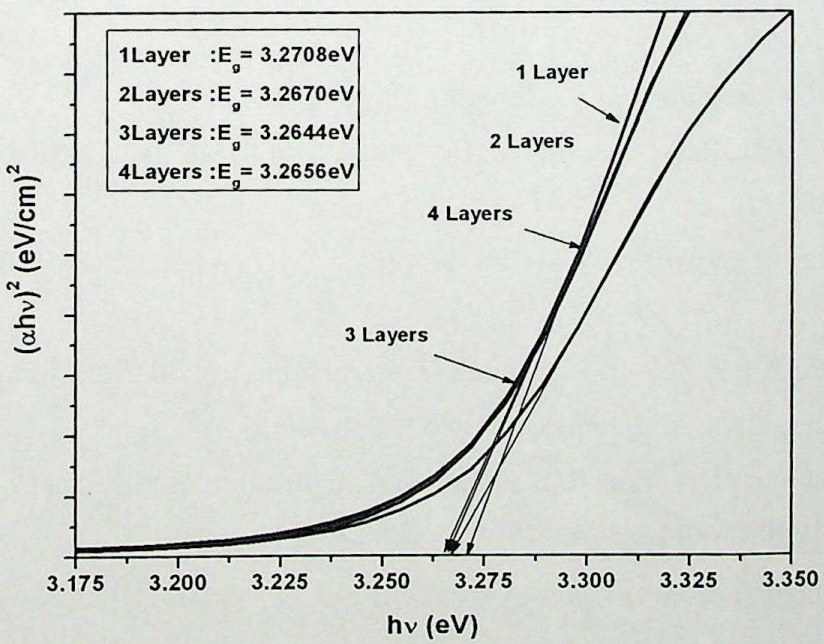


Figure 2.37: *The plot of $(\alpha h\upsilon)^2$ vs. $h\upsilon$ for different number of ZnO layers.*

References

1. P. S. Shewale, S. I. Patil and M. D. Uplane, Semicond. Sci. Technol. 25 (2010) 115008.
2. Chatwal G.R., Anand S.K., Instrumental methods of chemical analysis, Himalaya Publishing House (2006).
3. B. J. Lokhande, P. S. Patil and M. D. Uplane, Materials Letters 57 (2002) 573-579.
4. D. Zaouk, Y. Zaatar, R. Asmar, J. Jabbour, Microelectronics Journal 37 (2006) 1276–1279.
5. B. D. Cullity, Elements of X-ray Diffraction, Second ed., Addison-Wesley, Reading MA, (1978) 162.
6. Y. Caglar, S. Aksoy, S. Ilican, M. Caglar, Superlattices and Microstructures 46 (2009) 469-475.
7. S.S. Shinde, P. S. Patil, R.S. Gaikwad, R.S. Mane, B.N. Pawar, K.Y. Rajpure, Journal of Alloys and Compounds 503 (2010) 416–421.
8. S. J. Kang, Y. H. Joung, Applied Surface Science 253 (2007) 7330–7335.
9. J. George, M. K. Radhakrishnan, Solid State Commun. 33 (1980) 987.
10. T. Prasada Rao, M. C. Santhoshkumar, Applied Surface Science 255 (2009) 4579–4582.
11. S.-C. Chang, J. Vac. Sci. Technol. 17 (1) (1980) 366.
12. B. C. Yadav, R. Srivastava, C.D. Dwivedi, P. Pramanik, Sens. Actuators B 131 (2008) 216.
13. A. Jain, P. Sagar, R. M. Mehra, Materials Science-Poland, 25 (2007) 233-242.
14. P.S. Patil, P.K. Kawar, S. B. Sadale, Electrochim. Acta 50 (2005) 2527.
15. Mustafa Oztas, Chin. Phys. Lett. 25 (2008) 4090.
16. A. Ashour, M. A. Kaid, N. Z. El-Sayed, A. A. Ibrahim, Applied Surface Science 252 (2006)7844–7848.
17. B. J. Lokhande, M.D. Uplane, Appl. Surf. Sci. 167 (2000) 243.
18. S. M. Rozati, Sh. Akeste, Cryst. Res. Technol. 43(2008) 273 – 275.
19. Leon I. Maissel, Reinhard Glang, Handbook of Thin Film Technology part-2, McGraw- Hill

20. T. Prasada Rao, M. C. Santhosh Kumar, A. Safarulla, V. Ganesan, S. R. Barman, C. Sanjeeviraja, Physica B 405 (2010) 2226–2231.
21. M. Suchea, S. Christoulakis, M. Katharakis, N. Vidakis, E. Koudoumas, Thin Solid Films 517 (2009) 4303–4306.
22. S. S. Shinde, P. S. Shinde, S. M. Pawar, A. V. Moholkar, C. H. Bhosale, K. Y. Rajpure, Solid State Sciences 10 (2008) 1209-1212.
23. M. Sharma, R. M. Mehra, Appl. Surf. Sci. 255 (2008) 2527–2532.
24. M. Bouderbala, S. Hamzaoui, B. Amrani, Ali H. Reshak, M. Adnane, T. Sahraoui, M. Zerdali, Physica B 403 (2008) 3326–3330.
25. X. Yu, J. Ma, F. Ji, Y. Wang, C. Cheng, H. Ma, Appl. Surf. Sci. 245 (2005) 310–315.
26. B. D. Cullity, S. R. Stock, Elements of X-ray Diffraction, Prentice Hall, New Jersey, 2001, p. 619.
27. S. Ilican, Y. Caglar, M. Caglar, Preparation and characterization of ZnO thin films deposited by sol-gel spin coating method, J. Optoelectro. Adv. Mater. 10 (2008) 2578 – 2583.
28. J. M. E. Harper, Jr. C. Cabral, P. C. Andricacos, L. Gignac, I. C. Noyan, K. P. Rodbell and C. K. Hu, J. Appl. Phys. 86 (1999) 2518.
29. M. C. Santhosh Kumar, B. Pradeep, Semicond. Sci. Technol. 17 (2002) 261.
30. S.-S. Lin, J.-L. Huang, D.-F. Lii, Surface & Coatings Technology 190 (2005) 372–377.
31. M. Oztas, M. Bedi, Thin Solid Films 516 (2008)1703–1709.
32. F. Gao, S. P. Naik, Y. Sasaki, T. Okubo, Thin Solid Films 495 (2006) 68.